Final Report to the Joint Fire Science Program: *Project 09-1-04-2*

Sub-canopy transport and dispersion of smoke: A unique observation dataset and model evaluation

Principal Investigator and Corresponding author:

Tara M. Strand
NZ Rural Fire Research, Scion Research
Forestry Building, Forestry Road
Ilam, Christchurch 8041, New Zealand
Tara.Strand@scionresearch.com, +64 3 364 2987 ext 7954

Author's:
Miriam Rorig[1], Kara Yedinak[2], Dais Seto[3], Eugene Allwine[2], Francisco Alonso Garcia[4], Patrick O'Keefe[2], Veronica Cruz Checan[5], Robert Mickler[6], Craig Clements[3], and Brian Lamb[2]

Co-Investigator's:
Brian Lamb, Craig Clements, Miriam Rorig, Robert Mickler, and Harold Thistle[7]

[1]U.S. Forest Service, Seattle, Washington
[2]Washington State University, Pullman Washington
[3]San José State University, San Jose, California
[4]Universidad Metropolitana de Puerto Rico, San Juan, Puerto Rico
[5]Westat, Rockville, MD, was Universidad de Puerto Rico, Recinto de Rio Piedras, San Juan, Puerto Rico
[6] Alion Science and Technology, Durham, North Carolina
[7] U.S. Forest Service, Morgantown, West Virginia

Abstract

Low intensity prescription burning is used to reduce fuels, improve ecosystem health, and to mimic a natural fire pattern that is otherwise suppressed during the more intense wildfire season. There are many constraints that limit the ability to conduct prescribed burn operations, including (but not limited to) visibility reduction in transportation corridors, and compliance with National Ambient Air Quality Standards (NAAQS) for fine particulate matter (aerodynamic diameter ≤ 2.5 micrometers, $PM_{2.5}$) and ozone. There is a need for tools that predict potential smoke impacts so that prescribed burns can be carried out within the parameters of these constraints.

The *sub-canopy transport and dispersion of smoke* project was designed to collect a comprehensive dataset that would allow for the testing of the existing modeling pathways within the BlueSky Modeling Framework and, if needed, develop additional modeling pathways, for low intensity or smoldering fires. This project collected a unique set of data to characterize fire, turbulence surrounding the fire front passage, fuels, consumption, emissions, plume rise, and near-fire sub-canopy dispersion of smoke. The BlueSky Modeling Framework was tested at each modeling step to determine its capability to simulate smoke emissions and transport for these smaller fires. The Sub-canopy project has:

- o Collected turbulence data during fire front passage, pre- and post-burn fuel loadings, emissions, and smoke plume dispersion data from four low intensity prescribed burns that took place in five burn units;

- o Tested the existing wildfire default modeling path within the BlueSky Modeling Framework and additional pathways for use on predicting smoke emissions and dispersion from low intensity burns;

- o Used a Guassian line source model to test the capability of these types of models to simulate sub-canopy smoke plume transport near the fire-source;

- o Furthered understanding of turbulence produced by a ground fire underneath a forest canopy;

- o Collected extensive smoke plume concentration and emissions data;

- o Assisted with modifying the BlueSky Framework to include a new version of HYSPLIT and that gives access to HYSPLIT's particle-particle modeling mode; and

- o Outlined the best path through the Framework for operational use in low intensity burns.

The project has produced several scientific findings (see Section 3), however the main results are:

(1) An easy way to improve smoke emissions and dispersion predictions is to update the emissions factors algorithms used in the BlueSky Framework and in the default emissions model (FEPS). If the linear equations currently used are replaced with more recent equations and measured emission factors, predicted concentrations of CO, CO_2, CH_4, and $PM_{2.5}$ would be greatly improved.

(2) Adding an emissions module to the BlueSky Framework would allow for faster incorporation of the emissions research into real-time decision support tools as well as provide a means for using locally based emission factors (i.e., emissions from deep organic burning).

(3) $PM_{2.5}$ concentrations increased at all burns after sunset and during the smoldering phase. Ending ignition earlier in the day to allow for mixing and advection of smoke away from the forest floor would mitigate the amount of smoke trapped under the forest canopy and lower the potential for unwanted smoke impacts.

(4) A simple Gaussian line source model simulated near fire-source gas transport and dispersion, matching the observed maximum concentration. This model shows promise as a viable option for near-fire source smoke dispersion predictions.

(5) The BlueSky Framework v3.5 with the following path invoked is recommended for predicting smoke dispersion from low intensity fire. The model pathway is: observed fuel loads, where the pine litter fuel is placed in the 1-hr fuel category, Consumev3, FEPS, and HYSPLIT with particle-particle mode turned on. If fuel loads are not known, or if the fuel type that carries the fire is something other than litter, then FCCSv2 is recommended. Future improvements to the emissions step will hopefully improve the surface concentrations.

The objective of this study was to collect cohesive data set that represented low intensity fire smoke emissions and dispersion processes. The goal was to find a smoke modeling pathway within the BlueSky Framework that could be used operationally to predict smoke concentrations from low intensity burns. The methods used to collect the observation data, key observation findings, model-to-observation comparisons and management implications are described in the following sections.

Contents

1.   *Background and Purpose*

Many ecosystems within the United States (U.S.) require wildland fire to maintain ecosystem health and diversity (Bisson et al., 2003; Komarek, 1974). Unfortunately wildland fire is also a source of pollutant gas and particulate emissions that reduce visibility (Achtemeier, 2006) and degrade air quality (e.g., Chen et al., 2008; Strand et al., 2011). Small low intensity burns are used in the southeastern U.S. to reduce fuel loads, which mitigates wildfire risk, and restore ecosystem health (Glitzenstein et al., 2003). These small burns, usually less than 200 ha (500 acres) but sometimes as large as 400 ha (1000 acres), dominate the fire emissions landscape during the prescribed burning season of late autumn to early spring (Liu, 2004). Each small fire produces less smoke compared to that of a large wildfire and management of ignition time limits smoke emissions and local population exposure to smoke impacts. Nonetheless, region-wide summation of emissions from many small fires contributes to region-wide smoke impacts, sometimes resulting in prescribed burn restrictions.

Over the last decade smoke emissions, dispersion and air quality models have been developed to assist with predicting potential smoke impacts. One example is the BlueSky Modeling Framework (BlueSky Framework, Larkin et al., 2010), which was developed to link disparate models and data sets together to produce the inputs necessary to run the predictive smoke dispersion models. Many recent BlueSky Framework advancements have resulted in improved predictions during large wildfire events (Strand et al., 2012) and the BlueSky Framework is currently used operationally to assist with air quality forecasts for large wildfire incidents. In addition, recent research has allowed for further understanding of the uncertainty, limits, and strengths of the models within the BlueSky Framework (and others), in particular for large wildfire events (Larkin et al., 2012). Characterization of model pathway performance and predictions for smoke emissions and transport from small, low intensity fires has lagged behind the efforts aimed at the larger wildfire events. Lacking in recent smoke modeling advancements is the understanding of underlying BlueSky Framework model capabilities to predict smoke emissions, transport, and surface concentrations from small low intensity burns.

Observational data are required to evaluate model-pathway performance and/or to develop a new model/pathway. Historical data collection has focused on obtaining certain types of data (e.g., fuels only or surface concentrations only) and the majority of these datasets have not collected data from the same fire at each step within the smoke modeling pathway. This lack of same-fire cohesive observation data has hindered model uncertainty analyses and sensitivity studies (Larkin et al., 2012). The objective of this study was to collect a cohesive observation dataset that represented the smoke modeling emissions and dispersion pathway for low intensity/smoldering fires. Observations of fire, turbulence induced by fire front passage, fuel loadings, consumed fuels, emissions, and sub-canopy smoke dispersion were made at four low intensity burns in The Nature

Conservancy's Calloway Forest/Sandhills Preserve, North Carolina U.S. Where achievable, the data collection followed the Smoke and Emissions Modeling Intercomparison Project's (SEMIP) protocol (Larkin et al., 2012) for case study development. This allowed for comparisons of model output to observations at each smoke modeling output step within the BlueSky Framework. The methods used to collect the observation data, key observation findings, model-to-observation comparisons and management implications are described in the following sections.

2.   Study Description and Location

To improve low intensity smoke emission modeling capabilities, four observation datasets were collected before, during, and after four low intensity prescribed burns. Observation data of fire information, turbulence induced by fire front passage, fuel loadings, consumed fuels, emissions, plume rise, and sub-canopy dispersion of smoke were collected. The following subsections describe burn location, experimental design, and measurements made during the burns. Metric units are used to describe most variables; a conversion table is given in Appendix A.

2.1   Description of site and fuels

The experimental low intensity prescribed burns took place during the late winter and early spring (February and March) of 2010 and 2011 at The Nature Conservancy's (TNC) Calloway Forest/Sandhills Preserve in North Carolina (Fig. 1). Five burn units, with two burned on the same day, were used to collect observation data. Table 1 lists burn number, date it was burned, burn location and size and the start and end times of hand ignition.
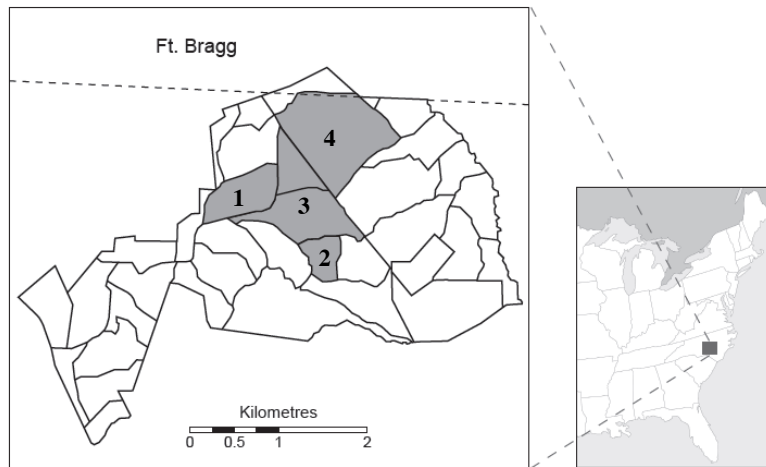
Figure 1. The experimental burns took place on The Nature Conservancy's North Carolina Calloway Forest/Sandhills Preserve. Five burn units (shaded dark grey), burned as four prescribed burns, and were used to collect data. Burn numbers are shown with their burn unit; burn 3 consisted of two units.

Table 1. Burn number, date the prescribed burn took place, size of the burn, start and end of hand ignition and the latitude and longitude in the center of the burn unit. Burn 3 was two burn units, which were burned in one day.

Burn #	Date	Latitude, Longitude	Size in acres (hectares)	Start of hand ignition (EST)	End of hand ignition (EST)
1	7-Mar-2010	35.03435, -79.28757	61 (25)	11:20 AM	3:20 PM
2	9-Mar-2010	35.02782, -79.27883	46 (19)	11:00 AM	2:45 PM
3	16-Feb-2011	35.03232, -79.28188	175 (71)	11:00 AM	5:00 PM
4	12-Mar-2011	35.03703, -79.27799	225 (91)	11:10 AM	3:00 PM

The Calloway Forest is a relatively uniform, approximately sixty-five years old, *Pinus palustris* Mill. (long leaf pine) stand. The forest sits on softly rolling terrain of old sand dunes resulting in sandy soil with little to no organic matter beyond the surface duff layer. The majority of the surface fuels were in the 1-hr size classification and consisted of long leaf pine litter, both cured and live wiregrass (*Aristida stricta*), American turkey oak (*Quercus laevis*), gallberry (*Ilex glabra*), regeneration long leaf pine in its bunch-

8

grass state and a small quantity of herbaceous species (Fig. 2). Surface fuels in the 10-hr and 100-hr size classifications were present however they were very few and did not carry the fire.

Figure 2. Pictures of the 1-hr surface fuels. Going counterclockwise, starting upper left, long leaf pine litter; lower left, regenerated long leaf pine in their bunchgrass state; and right wiregrass mixed with the pine litter, which was the fuel type that carried the fire.

2.2   Experimental design

Experimental set up was as consistent as realistically possible (Fig. 3) and was designed to collect internal (to the burn unit) fire front passage data along with external downwind plume concentrations. Several instrumented towers were deployed in and near the burn units. Two towers, 20 m in height, were equipped with sonic anemometers at 3 m, 10 m, and 20 m above ground level (AGL). The sonic anemometers measured winds in the three dimensions (N-S, E-W, and up-down) at a rate of 10 Hz (ten times per second) and were used to measure turbulence beneath the canopy and variation in wind direction before, during, and after the burn. To understand the vertical distribution of temperature during fire front passage, one tower was also equipped with an array of thermocouples placed every 1 m from ground level to 20 m AGL (burns 1 and 3) and to 10 m AGL (burn 4). Temperature data were sampled at 10 Hz and averaged to 5 Hz. The interior towers are named T1 for turbulence only (operated by the US Forest Service), and T2 for turbulence and temperature (operated by San José State University).

At the T2 tower, the total and radiative heat fluxes were measured. The sensors were mounted in a rectangular aluminum box and located near the towers, facing horizontally towards the fire front. Both the tower bases and heat flux sensors were protected from the extreme heat of the fire using fireproof insulation material. Seto (2012), Seto et al.

(2013), and Seto et al. (in preparation) describes the turbulence, buoyancy, and radiative flux methods of data collection in further detail.

Two 7 m meteorological towers, named MT1 and MT2, were deployed and equipped with temperature, relative humidity, and wind sensors at two levels, 1.2 m AGL and 7 m AGL. A net radiation sensor was also deployed at 1.2 m AGL. These towers were located near the experimental burns and collected standard surface sub-canopy meteorological data for the duration of the trials. A SOnic Detection and Ranging (SODAR) instrument was deployed near the burn units in a clearing and measured wind speed and direction every 15 minutes ranging from 0 to 200 m AGL. In the same clearing where the SODAR was located, rawinsondes were launched at the start and end of hand ignition to obtain vertical profiles of temperature, relative humidity, and winds from the ground to 10 km AGL. These data were used to determine atmospheric stability.

A 26 m tower was deployed downwind (burns 1 and 3) and within (burn 4) the burn unit and equipped to measure temperature, winds, turbulence, and gas concentrations. This tower was operated by Washington State University and is named TG. Four sonic anemometers were placed on the TG tower at 25.6 m, 19.7 m, 7.6 m, and 2.7 m AGL. A profiler measured temperature from eight heights ranging from 2.2 m AGL to 25.4 m AGL. The gases CO_2, CO, CH_4, NH_3, and H_2O were sampled at 25.6 m AGL (see Section 2.3.5 and Table 3). The sub-particle species BC and PPAH were sampled at 3 m AGL and the nitrogen species NO and NOx, from which NO_2 was computed, were sampled at 2.1 m AGL. The trace gases and particle concentrations were used to calculate emission factors and emissions. Post-trial analyses revealed the BC sensor was overwhelmed with high concentrations of particulate and performed poorly, therefore the data were dropped from analyses. See Yedinak (2013) and Yedinak et al., (in preparation) for further description on data collection and emission factor derivation.

Four to six $PM_{2.5}$ monitors were placed 50 m apart in a transect perpendicular to the expected mean wind direction at the base of the TG tower (burns 1, 3, and 4) or on the downwind burn perimeter (burn 2). The sample inlet was located 2.2 m AGL. Within the middle of the burn unit eight CO sensors were deployed every 50 m at 2.2 m AGL (burns 1, 3, and 4). For burn 2, CO sensors and $PM_{2.5}$ monitors were co-located on the downwind burn perimeter. Alonso Garcia (2012) further describes the deployment methods for the CO and $PM_{2.5}$ sensors.

Appendix B lists the micrometeorology sensors and the trace gas and particulate instruments, their manufacturers and the sampling rates.
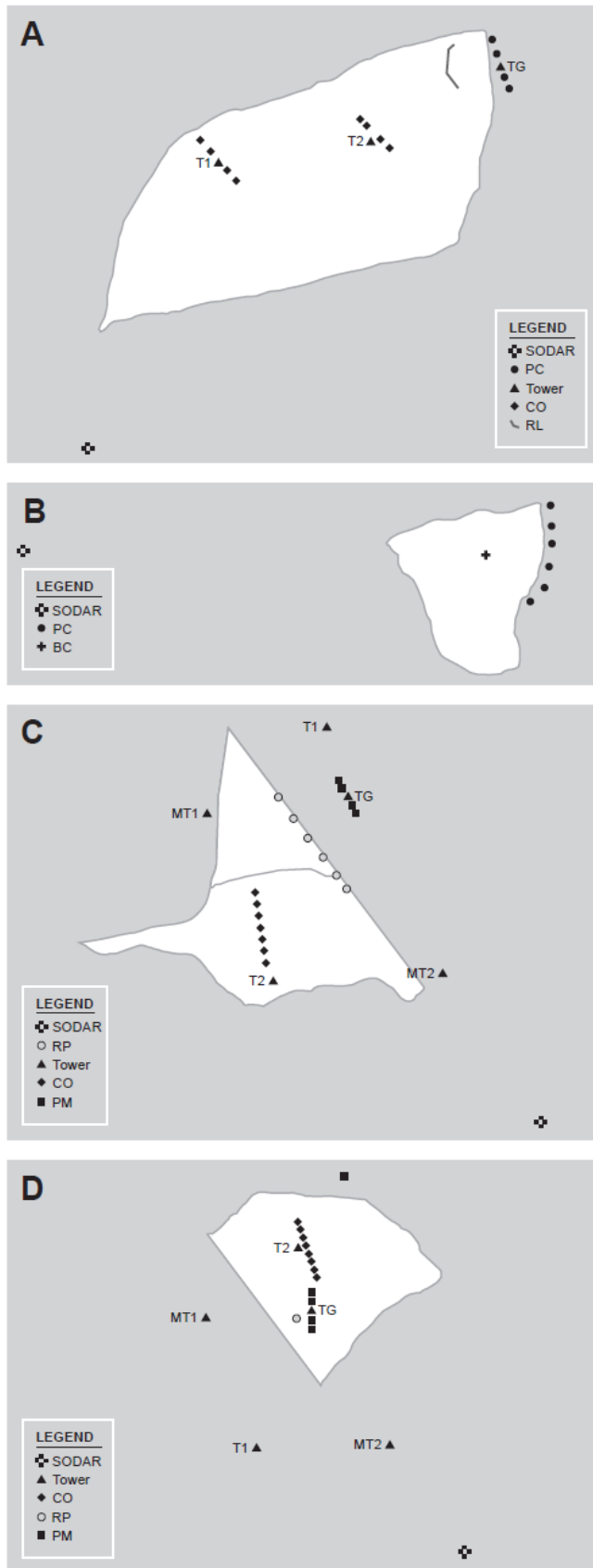
Figure 3. Experimental design for burn 1 (A), burn 2 (B), burn 3 (C), and burn 4 (D). Design changed based on meteorology, fire conditions, and instrument availability. The white area outlines the burn area. The triangles show where the tall instrumented turbulence (T1 and T2), trace gas (TG) and meteorological towers (MT1, MT2) were placed. For burn 1 and 2 the MT towers are off the map. The CO sensors are labeled CO and the $PM_{2.5}$ monitors are labeled PM. For burns 1 and 2 (A and B), the $PM_{2.5}$ monitors were co-located with CO sensors and these are denoted as PC. The grey line in burn 1 (A) shows the SF_6 line source, noted as RL, while the open circles show the SF_6 release points in burns 3 (C) and 4 (D), noted as RP. The SODAR and rawinsonde launch site are noted with the star. North is the top of the page.

2.3   Data collection

Observation data, where possible, were collected at the model output steps of the BlueSky Framework (Table 2). This was done to allow for model output-to-observation comparisons at each modeling step and at the end of the smoke modeling pathways. The observations collected at each burn differed slightly based on instrument availability, weather and conditions of the burn.

Instrument availability was limited for burn 2. It occurred two days after burn 1, the burn units were not contiguous and there was insufficient time to move the tall towers and the many sensors associated with the towers. Data collection was restricted to sensors that were portable. Alonso Garcia (2012) used $PM_{2.5}$ data collected from all of the burns, including burn 2, in his $PM_{2.5}$ and CO concentration analyses. Data from burn 2 helped to inform on the nighttime smoke plume movement and surface concentrations.

Table 2. Observation data were collected at the BlueSky Framework model output steps. Some burns lack data at some modeling steps this was due to instrument unavailability and weather and conditions surrounding the burn.

Model output step	Burn 1	Burn 2	Burn 3	Burn 4
Fire	X	X	X	X
Fuels	X		X	X
Consumption	X		X	X
Emissions	X		X	X
Plume rise			X	X
Dispersion	X	X	X	X

2.3.1 Fire information.

Fire information was recorded as location and area of the burn and start and cessation of ignition. This information was the basic fire-information input required by the BlueSky Framework. The note taker, via notification through hand held radios recorded location of hand ignition. For burn 4 a GPS unit was placed on an interior igniter to compare actual location to the verbal notification system. It was determined that the verbal notification system was comparable, particularly for the coarse level of fire location information used by the BlueSky Framework and other current smoke prediction models.

The predominantly flaming phase of the burn ceased shortly after hand ignition and was followed by smoldering/residual burning. For this study, the modified combustion efficiency (MCE) was used to determine when the burn was chiefly flaming or

smoldering (see section 2.3.5 for further details). A walkthrough after hand ignition ended allowed for a visual inspection and characterization of the burn phase, which was observed as smoldering.

2.3.2 Maximum fire temperature.

Maximum fire temperature was were observed using heat sensitive paints (Tempilaq®, Elk Grove Village, Illinois) that melted at 10°C (50°F) increments for temperatures that ranged from 93°C (200°F) to 538°C (1000°F). Aluminum tags consisting of pairs of racetrack numbered and un-numbered tags (Forestry Supplier Inc.) were painted with the heat sensitive paints. The painted tags were covered with a blank aluminum strip attached with a paper clip to reduce soot accumulations and enhance readability of the melting temperatures. This follows protocols found in the literature. The painted tags were set above the ground at the same height, 30 cm above the soil surface, along 30 m (100 ft.) north-south and east-west transects at 1 m intervals. Next to the interior CO sensor transect aluminum strips (10 x 30 cm) were painted with heat sensitive paints and co-located with tripod mounted air quality sensors.

Visible interpretation of the un-melted and melted paint was used to estimate the maximum temperature for each tag. The melting temperature interpretations were conducted by one person to reduce measurement error. This method has large uncertainty associated with it and is used to give a relative indication heat within the burn.

2.3.3 Fire rate of spread and flame height.

Fire rates of spread (burns 3 and 4) were estimated by placing 1 meter aluminum poles at a distance of 30.4 m (100 ft.) at a right angle to the prescribed fire ignition lines. The rate of spread was determined by visual inspection by the igniter using the video setting of a Nikon D3100 digital camera. The rate of spread was estimated when the head fire reached the pole and was joined by the backing fire at the opposite pole.

Flame heights were estimated using a 3 m (10 ft.) aluminum pole alternating painted with heat resistance white and black paint at 0.3 m (1 ft.). Flame height was determined by visual interpretation of the prescribed fire igniter and validated with video from the Nikon D3100 digital camera.

2.3.4 Pre and post burn fuels.

Prior to each burn ten plots were established for each vegetation type which consisted of four 7.3 m (24 ft.) radius subplots with a center plot and three subplots located at

azimuths of 0°, 120°, and 240°. Each subplot consisted of three transects and 2 m radius microplots, per Forest Inventory and Analysis (FIA) plot design, were surveyed, geospatial coordinates of the plots centers were collected using a Trimble®(XT, Sunnyvale, California) and plot centers and transect ends were pinned for relocation. One-hour fuels were characterized as litter, herb, and woody stems less than 0.25" in diameter. The litter was raked to bare earth and the shrubs, grasses, and other herbaceous species were clipped at the ground and placed in separate plastic bags. Ten-hour course woody debris, woody stems 0.26" to 1.0" were collected within the mircoplotsplot and placed in plastic bags. All one- and ten-hour fuel components were then weighed in the field utilizing a spring balance. Sample of fuels from each component were transferred to the lab in sealed plastic bags where they were first weighted, and then oven dried until sample weights remained constant and weighed on a top loading balance. Following weighing all wet and dried fuels components were returned to their respective microplots and distributed in a representative manner. Post burn biomass plots were relocated following prescribed burning using microplot GPS coordinates to locate microplot centers and transects. The charred/unburned one and ten-hour fuels within the microplot was raked and collected into plastic bags. The post burn fuels were weighed in the field using a spring balance and a sample of post-burn fuels were transferred to the laboratory, where they were weighed, oven dried, and weighed on a top balance to determine an oven dried weights. Post-burn fuels consisted of unburned and charred litter and ten-hour course woody debris.

Fuel moisture was measured by weighing the fuel prior to the burn and then brought to the lab where it was oven dried until there was no long a change weight. Fuel moisture was taken for each fuel type sub-class and litter, grass, 1-hr woody, etc., were separated out and weighed individually to obtain the mosaic of fuel moistures. The fuel moisture content was the difference in weight measured after oven drying from the wet weight measured and recorded in the field.

2.3.5 Concentrations and emissions.

Several gases and particle species were sampled before, during and after each of the prescribed burns (Table 3). Concentrations were recorded continuously and were used to derive emission factors and to determine smoke plume transport and dispersion behavior. Further description of methods can be found in Yedinak (2013) and Yedinak et al., (in preparation). The instruments that were used and their sampling rates can be viewed in Appendix B.

Table 3. Lists of trace gases and particles species measured during each burn and location of the instrument relative to the burn.

Burn Number	Gas and particle species measure[*]	Location relative to burn
1	CO_2, CO, NO, NOx, $PM_{2.5}$, BC, PPAH	All were measured downwind at TG CO was also measured within the burn
2	CO $PM_{2.5}$, BC	$PM_{2.5}$ and CO were measured downwind BC was measured within the burn
3	CO_2, CO, CH_4 NO, NO_2, NH_3, N_2O $PM_{2.5}$, BC, PPAH	All were measured downwind at TG CO was also measured within the burn
4	CO_2, CO, CH_4 NO, NO_2, NH_3, N_2O $PM_{2.5}$, BC, PPAH	All were measured within the burn at TG

[*]Full name and acronyms in parenthesis for each gas and particle species listed: Carbon dioxide (CO_2), Carbon monoxide (CO), Methane (CH_4), Nitrogen oxide (NO), Nitrogen dioxide (NO_2), NOx represents $NO+NO_2$, Ammonia (NH_3), Fine particulate matter (aerodynamic diameter ≤ 2.5 micrometers, $PM_{2.5}$), Black carbon (BC), and Particle-bound polycyclic aromatic hydrocarbons (PPAH).

Gas and particulate concentrations were used to derive emission factors, which were then used to calculate observed emissions. To calculate the emission factors, the Ward and Radke (1993) carbon balance method further defined by Yokelson et al. (1999) was used in the following manner:

$$EF_x = F_c \times 1000 \ (g \ kg^{-1}) \times \frac{\Delta X}{\Delta C_t}, \qquad (1)$$

where EF_x is the emission factor for compound X (g species emitted per kg of fuel consumed). The carbon mass fraction (F_c) of the fuel (g carbon per g of fuel) was assumed to be 0.5 for this study and was based on the summary provided by Urbanski et al. (2008). ΔX was the excess concentration of species X and ΔC_t was the sum of excess carbon concentrations of CO_2, CO, CH_4 and $PM_{2.5}$. The carbon content of $PM_{2.5}$ was conservatively assumed to be 50% compared to work by Burling et al. (2011) and Ferek et al. (1998) who estimated carbon mass fractions of 69% and 75% respectively. Figure 4 walks through the method used to calculate emissions from observations.
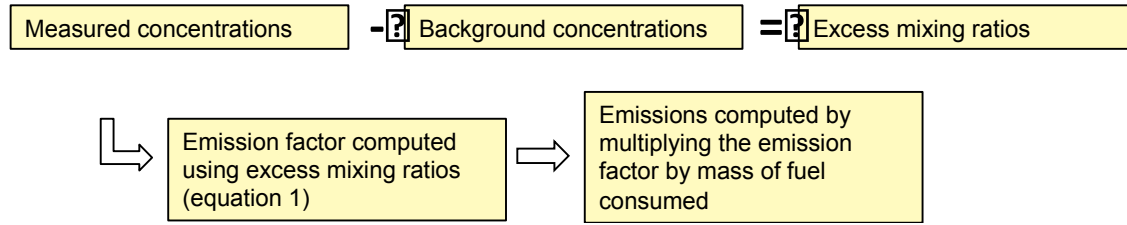
Measured concentrations	**-**	Background concentrations	**=**	Excess mixing ratios

Emission factor computed using excess mixing ratios (equation 1)	Emissions computed by multiplying the emission factor by mass of fuel consumed

Figure 4. Schematic of how emissions are computed from measured concentrations.

Modified combustion efficiency, equation (2), was used to determine if the derived emission factors were from the predominantly flaming or smoldering phases of the burn.

$$MCE = \frac{\Delta CO_2}{\Delta CO_2 + \Delta CO},\qquad\qquad(2)$$

where ΔCO_2 and ΔCO are the excess mixing ratios. Following Akagi et al. (2011) emissions associated with an MCE < 0.9 are considered predominantly smoldering emissions while emissions with MCE > 0.9 are associated to the flaming phase. Emissions associated with an MCE value of 0.99 are considered pure flaming.

2.3.6 Plume rise.

Above canopy plume rise was measured from an open field, near the SODAR site, located 1.5 km to the east of the burns and relatively perpendicular to the mean plume direction. This location provided a good view of the plume characteristics, such as plume top, angle, and smoke color. An inclinometer was used to measure the plume top throughout the duration of the burn (burns 3 and 4) and these values were recorded along with comments on general plume behavior.

2.3.7 Released trace gas.

The trace gas sulphur hexafluoride (SF_6) was released from within the burn and was measured downwind at the TG tower through four inlets placed at 25.6 m, 19.7 m, 13.3 m, and 2.7 m AGL. The gas was released from a 100 m line source (burn 1), 6 point sources (burn 3) or 1 point source (burn 4). The release method changed depending on the burn size and distance between the release points and TG. The SF_6 data (burns 1 and 3) were used to test a line source model for possible application of predicting smoke plume transport and dispersion from low intensity prescribed burns.

2.4   Model predictions

The BlueSky Framework was used to model fuel loadings, fuels consumed, emissions, plume rise, and surface concentrations of $PM_{2.5}$. At the time of this study the default pathway through the BlueSky Framework (v3.0) was considered one of the best smoke emissions/dispersion modeling pathways and several regional and national smoke prediction tools were using the default pathway to produce their output. The individual component models used within the default pathway are listed in Table 4 (grey shade).

To quantify model/pathway performance and to determine the best model for low intensity burns, model predictions at each output level were compared to observations and to a tuned version of the model. To 'tune' the model, observations were used in the modeling pathway one step prior to the output comparison level. For example observed fuel consumption was used to tune the FEPS emissions model, which computed emissions. The 'tuned' results were used to examine if using observations instead of models in the earlier steps of the smoke modeling pathway could improve model output. The results, named 'tuned', were compared to the observations and the pure model output. Table 4 lists the comparisons made at each modeling step.

Table 4. Models tested, including those that were in the default pathway (BlueSky Framework v3.0, grey shade), to find the best smoke modeling pathway for low intensity prescribed burns. 'Tuned' refers to using observations in earlier modeling steps to replace model output.

Model step	*Models tested*
Fuel Loading	FCCS v1[a], FCCS v2[b], Observations
Total Consumption	Consumev3[c], Tuned F1, Tuned F2, Observations
Emissions	FEPS[d], Tuned F1, Tuned F2, Tuned C, Observations
Plume Rise	FEPS, Tuned F1, Tuned F2, Tuned C, Observations
$PM_{2.5}$ Surface Concentrations	HYSPLIT[e], CALPUFF[f], Tuned F2

[a]1-km gridded data Mickenzie et al. (2007) [e]Draxler (1999)
[b]50-m gridded data [f]Scire et al. (2000)
[c]Prichard et al. (2010)
[d]Anderson et al. (2004)

Meteorological model.

The dispersion model step requires four dimensional meteorological gridded fields, which were generated by USDA Forest Service Northern Research Station using the Pennsylvania State University/National Center for Atmospheric Research Mesoscale

Model, Version 5 (MM5) v3.7 (Grell et al., 1994). A 1.33 square km horizontal grid with 109 east-west and 109 north-south cells was used to generate hourly predicted meteorological data over TNC Calloway Forest. Vertically, 35 layers were used with the upper levels closely spaced within the boundary layer and decreasing in resolution (spaced farther apart) above the boundary layer, extending to 100 mbar. Surface concentrations of $PM_{2.5}$ were predicted on a domain that encompassed TNC Calloway Forest using the same horizontal grid as the modeled meteorological data.

Initial and boundary conditions were derived from the National Centers for Environmental Prediction (NCEP) North American Mesoscale (NAM) model 40 km forecast product (Janjic, 2003) and the Eta Mellor-Yamada planetary boundary layer scheme (Janjic, 1990, 1994) was implemented to further describe the boundary layer. Other parameters set within the MM5 model include the Rapid Radiative Transfer Model (RRTM) longwave radiation scheme (Mlawer et al., 1997), the Kain-Fritsch cumulus parameterization (Kain and Fritsch, 1990), the MM5 cloud-radiation scheme for shortwave radiation (Dudhia, 1989) and the Dudhia simple ice explicit moisture scheme (Dudhia, 1996).

3.   *Key findings*

In this section we present key observation data followed by model comparison results. Results from a Gaussian line model, which was used to simulate sub-canopy plume dispersion near the fire-source, are also presented and the Gaussian puff model used as a virtual laboratory is explored. For further details and results, please refer to Alonso Garcia (2012), Seto (2012), Seto et al. (2013), Seto et al. (in preparation), Yedinak (2013), and Yedinak et al (in preparation). A final paper (Strand et al., see Table 10) that summarizes the model comparison results will be available after December 2013.

Key findings are presented below in each sub-section.

3.1   Basic meteorological conditions

Basic weather observations were used to determine non-fire related meteorology, atmospheric stability and local vertical wind profiles. Relative humidity was lowest during burn 1, at 20% before ignition and ranging 13% to 18% during the burn, and highest during burn 3, at 30% before ignition and ranging from 35% to 40%. Relative humidity before burn 4 was 25% before ignition and ranged from 20% to 35% during ignition.

Wind speeds at the surface were similar for all burns ranging from < 5 m s^{-1} (burn 1), 1 and 3 m s^{-1} (burn 3), and 1 to 6 m s^{-1} (burn 4). Wind direction varied from burn to burn

because specific wind directions were needed for each burn to collect trace gas and particulate data. The observed mixing heights prior to ignition for burn 1, burn 3, and burn 4 were ~1.5 km (Fig. 5a) above ground level (AGL), ~1 km AGL (Fig. 5b), and ~0.6 km AGL (Fig. 5c), respectively.

- An unstable layer (superadiabatic layer) was observed near the ground for all burns.

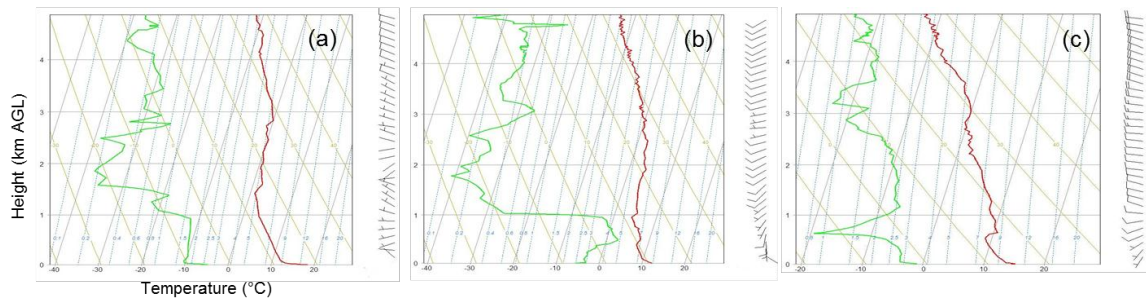- Atmospheric conditions were dry for all burns.

Figure 5. Sounding profiles of temperature (red), dew point (green), and wind speeds and directions (vectors on the right side) plotted with height and observed prior to the ignition at: (a) 11:11 EST for burn 1, (b) 11:18 EST for burn 3, and (c) 11:21 EST for burn 4. Note the temperature scale for (c) varies from that used for (a) and (b). Lines of constant temperature, dry adiabat, and saturation mixing ratio are also shown in the background. Data up to 5 km AGL presented, however data were collected up to 10 km AGL.

3.2   Fire data and information

We define fire temperature as the temperature experienced by the paints due to exposure to the fire and the heated fire environment. The temperature paints provide a maximum temperature value to the lowest 50°F interval. For burn 3, the median maximum fire temperature was 550°F with a range from 250°F to 650°F. There was one location from the CO sensor transect that experienced temperatures in excess of 1221°F (660°C). This known because the aluminum sheeting holding the paint chips melted. The melting point of aluminum is 660°C so we know the sheeting was at least heated to this point. This high temperature was a result of proximity to gallberry shrub vegetation which had intense fire behavior for a short duration. Burn 4 was an overall cooler burn with a median maximum fire temperature of 350°F and a range from 200°F to 1000°F.

Maximum flame height ranged from 1.5 m (4.9 ft., burn 4) to 1.8 m (5.9 ft., burn 3). From Pearce et al. (2012) and Alexander (1982), assuming little to no wind, a flame height of 1.2 m produces 386 kW/m fire intensity while a flame height of 1.8 m results in

933 kW/m fire intensity. Fire intensity during burn 3 was at least two times greater than fire intensity during burn 4.

The average fire-front rate of spread for burn 3 was 0.14 m/s (0.46 ft/s) and 0.37 m/s (1.21 ft/s) for burn 4. The rate of spread for burn 3 was slower and the hand ignition was longer, lasting 6 hours verses the 4 hours to complete burns 1, 2, and 4.

- The fire environment conditions dictated a slower ignition pace for burn 3; timing of emissions was therefore longer than otherwise expected and predicted by the BlueSky Framework.

- The slower ignition of burn 3 generated a greater extent of mixed emissions from the flaming and smoldering phases within the smoke plume (see Fig. 9).

- The differences between burn 3 and burn 4 are good reminders that small changes in flame height can lead to large changes in fire intensity, which in turn effects the emissions (e.g., NOx is formed at higher combustion temperatures).

3.3 Fire front passage and turbulence

In this section the changes in the horizontal and vertical winds on a fine temporal scale are discussed. Further details and discussion of turbulence during fire front passage (FFP) can be found in Seto (2012) and Seto et al. (2013). Seto et al. (in preparation) found sub-canopy turbulence to increase during the FFP and then quickly return to pre-FFP conditions. Majority of the turbulence and therefore recirculation and mixing occurred below the mid-canopy height (10 m, 33 ft.).

3.3.1 Horizontal wind speeds.

For all burns the average horizontal winds increased during FFP at all heights (Fig. 6). For burn 1, at tower T1, the winds at the canopy top slightly increased, conversely winds measured at the canopy top at the T2 towers (burns 1 and 3) increased considerably. On average the FFP increased the average wind speeds near the forest floor by 0.8 m s^{-1} (burn 1, T1), 1.0 m s^{-1} (burn 1, T2) and 1.2 m s^{-1} (burn 3, T2).

- The increased horizontal winds ranged from the forest floor to the canopy top and this demonstrates that even a surface fire with average flame heights of 1.5 m to 1.8 m will influence air movement at the canopy top, 20 m (66 ft.) above the ground.

- The inflection, lower wind speeds caused by canopy drag, typically observed below a forest canopy, was also observed during the FFP, which suggests that winds induced by the FFP were not strong enough to completely overcome canopy drag.
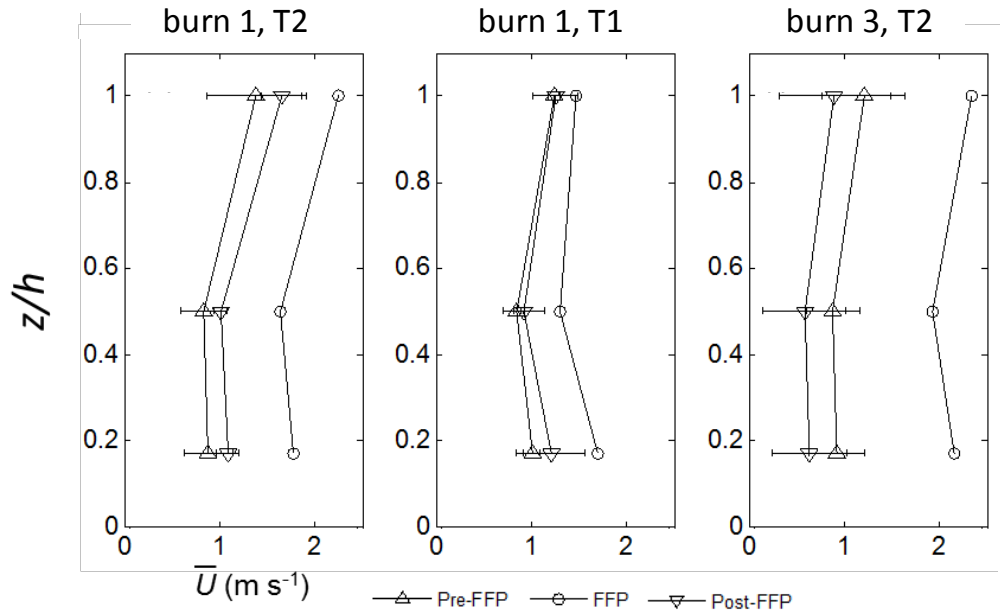
Figure 6. Average wind speeds (horizontal winds) recorded at the T1 and T2 towers during burns 1 and 3 at all three heights. The height has been normalized to the canopy top (20 m, 66 ft, or *z/h = 1*). The winds prior to (triangles) and after (upside down triangles) fire front passage are shown with winds during fire front passage (circles). The error bars represent 1 standard deviation.

3.3.2 Vertical wind speeds.

The vertical wind velocity (up-down motion) is an indicator of the strength of the smoke plume's buoyancy. There was considerable increase in vertical velocity during the FFP due to the buoyant motion produced by the FFP (Fig. 7). Majority of the upward velocities were on an order of 5 m s^{-1} (11 mph) with the strongest updraft of approximately 8 m s^{-1} (18 mph) observed near the canopy top during burn 3 at T2. Increased downdraft strength was also evident during the FFP and on average the downdraft strength was < 5 m s^{-1} (<11 mph).

- The downdrafts occurred mainly within the canopy, rather than pulling in air from above-canopy. Isolated within canopy circulation may have pre-heated the fuels faster than otherwise expected, increasing the quantity of fuels available to burn.
- The strongest measured updraft occurred concurrently with a peak in sonic temperature during the FFP (burn 3, T2). The magnitude of this updraft is large for a low-intensity burn and is indicative of the strength of wildfire updrafts.
- Vertical wind speeds carry emissions up and away from the ground or down towards the ground. Their strength is a measure of near fire mixing and plume dilution.
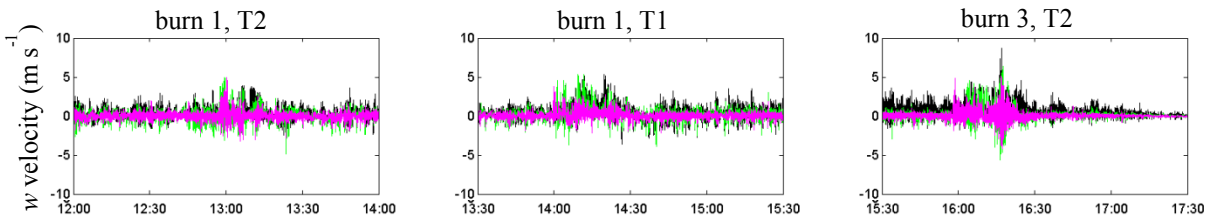
21

Figure 7. Time series (EST) of 10 Hz vertical wind speed observed at T1 and T2 during burns 1 and 3. The black, green, and pink colors represent values measured at 20 m, 10 m, and 3 m AGL, respectively. The period fire was close to the tower was centered on: 13:05 for burn 1, T2; 14:10 for burn 1 T1; and 16:15 for burn 3 T2.

3.3.3 Plume thermodynamics.

Temperature varied with height during FFP (Fig. 8) signifying rapid mixing between the ground and the canopy top. In some instances elevated temperatures were only observed in a middle layer ranging from 3 m to 8 m (9.8 ft. to 26 ft.), see Fig. 8a. A maximum average temperature was recorded during burn 3 at T2 near the canopy top (Fig. 8b). Coinciding with this maximum was a strong updraft near the forest floor and mid-canopy (Fig. 8, Arrow C), implying strong buoyant tendencies during this phase of the FFP.

Intrusion of cool air to the surface was observed during FFP and the downdrafts (vertical velocity) exceeded the ambient velocities. The arrows A and B in Figure 8 show an example of this intrusion.

- Strong downdraft wind speeds were not observed at the canopy top during FFP, although strong downward velocities were recorded at the 10 m (33 ft.) height.
- This supports the hypothesis that majority of the fire induced turbulence and recirculation was between the forest floor and mid-canopy.
- Strong buoyant tendencies are associated with rapid plume rise and higher plume tops.
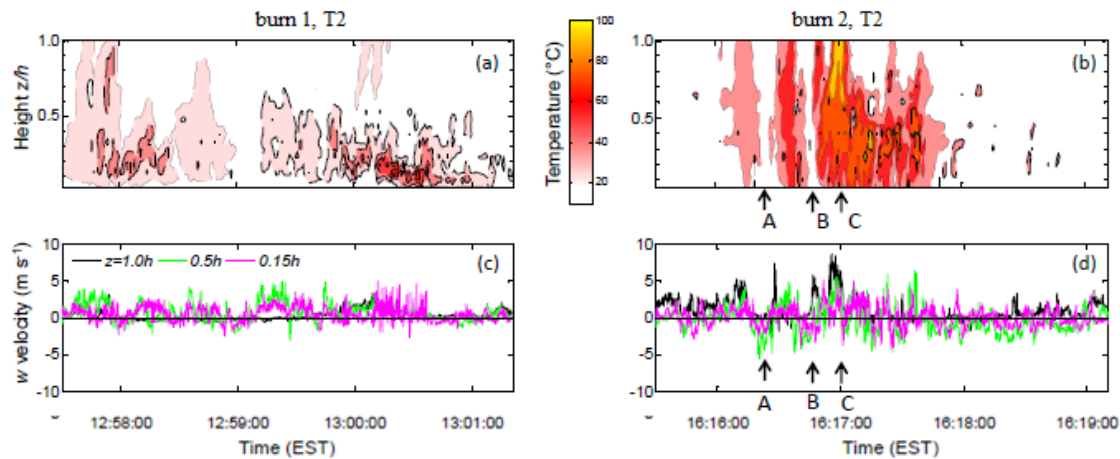
Figure 8. Time-height plot of 1-second averaged temperatures during fire front passage (top), and time series of 10 Hz in-plume vertical wind speed velocity (bottom). The black, green and pink colors represent vertical wind speeds at 20 m, 10 m and 3 m AGL, respectively. The Arrows A, B, and C highlight examples of colder air intrusion (A and B) and strong buoyancy (C).

3.4 Fuels and consumption

Pre-burn fuel loadings were 7,039 kg/ha (3.14 tons/acre, burn 1), 13,024 kg/ha (5.81 tons/acre, burn 3), and 11,993 kg/ha (5.35 tons/acre, burn 4). The pre-burn fuel loadings differed due to the managed fire return interval over the previous ten years, with burn 1 having an average fire return interval of 2 years and burns 3 and 4 with 2.6 and 3 years, respectively. Prescribed burns 1 and 4 consumed similar amounts of fuel relative to their pre-burn fuel loads, 73% and 67%, respectively. Corresponding post fire fuel loads were 1928 kg/ha (0.86 tons/acre) for burn 1 and 3945 kg/ha (1.76 tons/acre) for burn 4. Remaining fuel in burn 3 was 1928 kg/ha (0.86 tons/acre) with 85% of the fuel consumed.

The average overall fuel moisture content (FMC) does not explain the higher quantity of fuel consumed during burn 3. The average FMC, across all fuel types, was 35%, 38%, and 26% for burns 1, 3, and 4, respectively. A higher percentage of fuel burned during burn 3; in addition, the management of burn 3 was difficult compared to burns 1 and 4. (Note: The relative humidity was also higher during burn 3 compared to burns 1 and 4.)

- The higher fuel consumption observed for burn 3 was associated to the low fuel moisture of the wiregrass fuel type, which was (20%) compared to burns 1 (24%) and 4 (23%). Wiregrass was one of the primary fuels that carried the fire.

- The sub-class fuel types that principally carry the fire may dictate overall burn behavior and are important to consider for fire behavior assessment, heat intensity, and emissions calculations.

- The speciated emissions will vary depending on the fire intensity.

3.5   Surface concentrations

Excess surface concentrations of the sampled gases and particulates increased during the burns. For burn 3 the maximum excess concentration for all trace gases occurred during hand ignition whereas the maximum $PM_{2.5}$ excess concentration occurred after ignition (Fig. 9). For burn 4 the maximum excess concentration values for both $PM_{2.5}$ and the trace gases occurred when hand ignition surrounded the TG tower (Fig. 10). The magnitude of the excess concentrations varied between burns due to the proximity of the TG tower to the fire source. The TG tower was 500 m downwind from the edge of burn 3 and within burn 4, hence the transport time from the fire emissions source to TG varied. Plume age at TG during burn 3 ranged between 2 and 10 minutes verses 0 and 3 minutes during burn 4. Trace gas and particulate excess concentrations are described in detail in Yedinak (2013) and Yedinak et al. (in preparation).

- Excess concentrations of CO_2 (burns 3 and 4), CH_4 (burns 3 and 4), and NO_X (burn 4) were strongly correlated to CO during the flaming phase (MCE > 0.9).

- NH_3 is a smoldering product emitted when combustion is inefficient. NH_3 concentrations were correlated well with CO during the smoldering phase (MCE < 0.9) of the burn but not during the flaming phase.

- MCE fluctuated frequently during burn 3 (Fig. 9) compared to burn 4 (Fig. 10), we hypothesize that this is due to the slower ignition and therefore and increased mixing of smoldering and flaming emissions.

The pattern of observed $PM_{2.5}$ concentrations was similar across all four experimental burns and can be broken down into three phases: initial peak, concentration fluctuations, and elevated nighttime concentrations. The initial concentration peak occurred when burn ignition was close to the monitor locations, and for burns 1 and 4 this was when the maximum was recorded. Concentration fluctuations occurred as ignition progressed away from the monitors and were caused by plume meander and dilution. Concentrations began to increase between 17:00 and 18:00, shortly after ignition ceased, and remained elevated, ranging in the hundreds to low thousands ($\mu g/m^3$), until 24:00 (Fig. 9, bottom). For burns 2 and 3, maximum $PM_{2.5}$ concentrations were recorded during this period. $PM_{2.5}$ concentrations measured during all four burns are discussed further in Appendix C along with a comparison between E-Sampler and EBAM data collected during burns 3 and 4. $PM_{2.5}$ concentrations and their trends are also described by Alonso Garcia (2012).

The sub-particles, PPAH followed a similar to trend to $PM_{2.5}$ during burns 3 and 4. PPAH are emitted during combustion and elevated concentrations indicate that the plume came from a combustion source.

- Timing of the elevated nighttime $PM_{2.5}$ concentrations corresponds to the development of the nocturnal boundary layer, which enhanced the canopy barrier affect; trapping the plume under the canopy and prohibiting plume mixing and diluting.

- The monitors for burns 1, 2, and 3 were located down a very slight hill and nighttime drainage advected the smoke trapped under the canopy to the monitor locations.
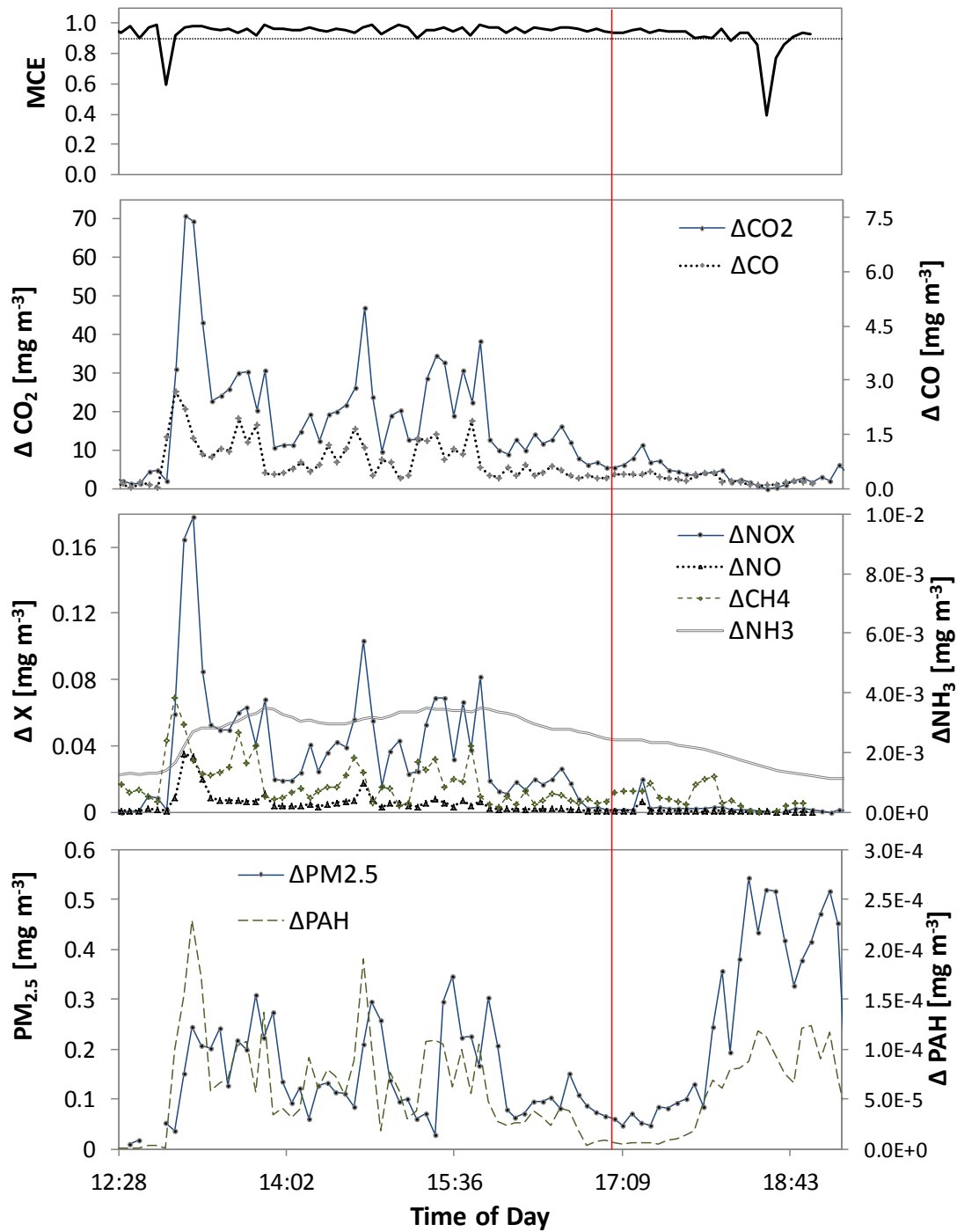
Figure 9. The 5-minute averaged time series of MCE and excess concentrations of CO, CO_2, NO_X, NO, CH_4, NH_3, $PM_{2.5}$, and PPAH (noted as PAH) for burn 3 (16-Feb-2011). The time series starts when the smoke plume first encounters the tower and the red vertical line denotes the end of the prescribed burn hand ignition. Note an MCE > 0.9 is usually considered the primarily flaming phase while MCE < 0.9 is the predominantly smoldering phase.
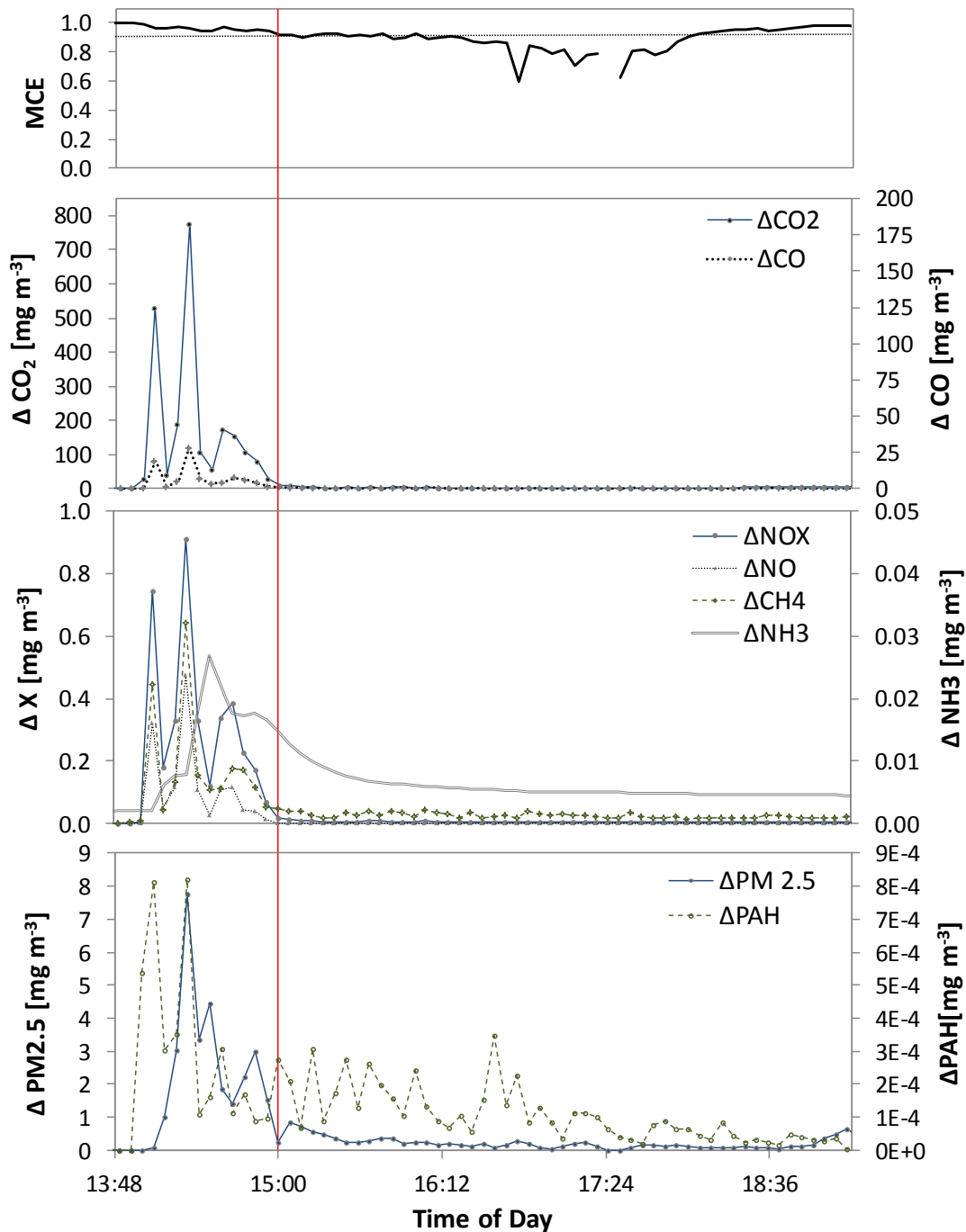
Figure 10. The 5-minute averaged time series of MCE and excess concentrations of CO, CO_2, NO_X, NO, CH_4, NH_3, $PM_{2.5}$, and PPAH (noted as PAH) for burn 4 (12-Mar-2011). Scales differ between Figures 9 and 10. The time series starts when the smoke plume first encounters the tower and the red vertical line denotes the end of the prescribed burn hand ignition. Note, an MCE > 0.9 is usually considered the predominantly flaming phase while MCE < 0.9 is the primarily smoldering phase.

3.6   Emissions

Emission factors (EF) of CO, CO_2, CH_4, NO_X, NO, NH_3, $PM_{2.5}$ and PPAH were calculated for burns 3 and 4 (Table 5). Due to the semi-quantitative nature of the PPAH sensor, the PPAH values are more uncertain than the other species, but provide information on the relative emission rate compared to other emitted species.   The key features of the EF results include:

- The magnitude and variability between flaming and smoldering periods in the emission factors of CO, CO_2, CH_4, NO_X, and NH_3 are within the ranges reported in the literature for U.S. based emissions.

- The average derived EF for $PM_{2.5}$ is at the upper limit of what has been previously reported in the literature for EF derived from observations made at U.S. based prescribed fires. The smoldering EF is above what has been previously reported either as mixed emissions or smoldering emissions.

- Though within the bounds of previous work, the emissions factors of the measured nitrogen containing species (NO_X and NH_3) were both on the high end of the reported range.

- There were considerable increases in emissions for some species (CO, CH_4, NO, and NOx), between burn 3 and burn 4 which may be related to a more efficient combustion during burn 3.

For the nitrogen species, NO and NOx emissions were lower in burn 4 verses burn 3, but NH_3 emissions were higher. This suggests that burn 3 was hotter, since NOx is formed at higher temperatures, and that there was less smoldering, indicated by the lower NH_3 emissions. NH_3 is a smoldering nitrogen product. There was basic visual observation of increased 'green' in the fuel bed between burns 3 and 4 and this may have contributed to the differences in burn emissions. The greening was not just noted visually, the long leaf pine seedlings and wiregrass increased in fuel moisture between burns, despite an overall decrease in average fuel bed moisture.

As expected, the EF derived during the flaming phase for CO was strongly correlated to MCE, however the EF derived for CO_2 did not demonstrate as high a correlation (Fig. 11), suggesting the excess concentrations of CO played a dominant role in the MCE and emission factor equations. This was reduced for burn 4, when the fire front passage was directly below the tower.

Consistent linear relationships are important because they can be used within models as generic algorithms to predict emission factors. The linear relationships between the derived CO EF and MCE for burns 3 and 4 are similar, indicating good potential for use in models; interestingly, this is also true for CO_2, despite the mediocre correlation to MCE. Derived emission factors for $PM_{2.5}$ displayed a poor relationship with MCE.

Derived emission factors for NO_X and NO were poorly correlated to MCE and NH_3 was poorly correlated in the flaming phase, but highly correlated to MCE in the smoldering phase. Please refer Yedinak (2013) and Yedinak et al. (in preparation) for further details.

Table 5. Derived emission factors for burns 3 and 4. These factors were used to compute total emissions. There is high level of uncertainty in the PPAH values. The N value represents number of 5-min average values that went into the calculation. There were two approaches to define the flaming and smoldering phases: (i) Use MCE and the > 0.9 threshold as the flaming phase; and, (ii) Use the visual observations of no known visible flames remaining.

Burn 1	MCE > 0.9			MCE < 0.9			Visible Flame			Post Ignition			Overall	
	#	avg	(±)	#	avg	(±)	#	avg	(±)	#	avg	(±)	avg	(±)
MCE	53	0.97	(0.03)	26	0.76	(0.17)	57	0.93	(0.07)	22	0.782	(0.19)	0.89	(0.13)
CO_2	53	1693	(145)	27	1068	(378)	58	1605	(189)	22	1005	(366)	1440	(366)
CO	53	52.9	(41.8)	27	302	(206)	58	112	(102)	22	256	(193)	152	(147)
CH_4	52	4.3	(6.3)	26	15.8	(28.5)	58	4.9	(8.3)	20	7.8	(6.0)	5.7	(7.85)
NO_X	48	4.8	(3.6)	17	1.77	(1.38)	58	4.1	(3.1)	8	3.2	(5.6)	3.98	(3.47)
NO	48	0.91	(1.06)	17	0.76	(0.88)	58	0.84	(0.84)	8	1.18	(1.89)	0.88	(1.01)
NH_3	53	0.38	(0.40)	27	2.12	(1.50)	58	0.68	(0.71)	22	2.03	(1.60)	1.06	(1.19)
PPAH	47	0.006	(0.002)	17	0.004	(0.003)	57	0.006	(0.004)	8	0.004	(0.003)	0.006	(0.003)
$PM_{2.5}$	46	19.4	(13.0)	16	45.0	(32.0)	54	23.2	(19.2)	8	44.0	(34)	25.9	(22.4)

| Burn 2	MCE > 0.9			MCE < 0.9			Visible Flame			Post Ignition			Overall	
	#	avg	(±)	#	avg	(±)	#	avg	(±)	#	avg	(±)	avg	(±)
MCE	39	0.99	(0.02)	24	0.82	(0.08)	16	0.96	(0.02)	47	0.88	(0.08)	0.90	(0.08)
CO_2	39	1773	(122)	24	1185	(317)	16	1670	(107)	47	1309	(280)	1647	(244)
CO	39	17.8	(37.0)	24	230	(74.9)	16	60.1	(40.6)	47	166	(87.9)	53.4	(78.7)
CH_4	39	2.84	(2.97)	24	24.1	(15.5)	16	3.06	(2.75)	47	18.0	(13.5)	6.89	(9.14)
NO_X	37	1.51	(1.25)	24	1.20	(0.49)	14	2.71	(1.29)	47	1.00	(1.29)	1.39	(1.02)
NO	37	0.40	(0.44)	24	0.27	(0.13)	14	0.81	(0.48)	47	0.21	(0.48)	0.35	(0.35)
NH_3	39	0.53	(1.07)	24	5.30	(4.14)	16	1.13	(1.77)	47	4.12	(3.41)	1.41	(2.41)
PPAH	37	0.009	(0.008)	24	0.019	(0.010)	14	0.004	(0.004)	47	0.015	(0.004)	0.013	(0.010)
$PM_{2.5}$	36	27.1	(20.0)	23	36.8	(23.4)	13	30.3	(24.1)	46	31.1	(24.1)	30.9	(21.7)
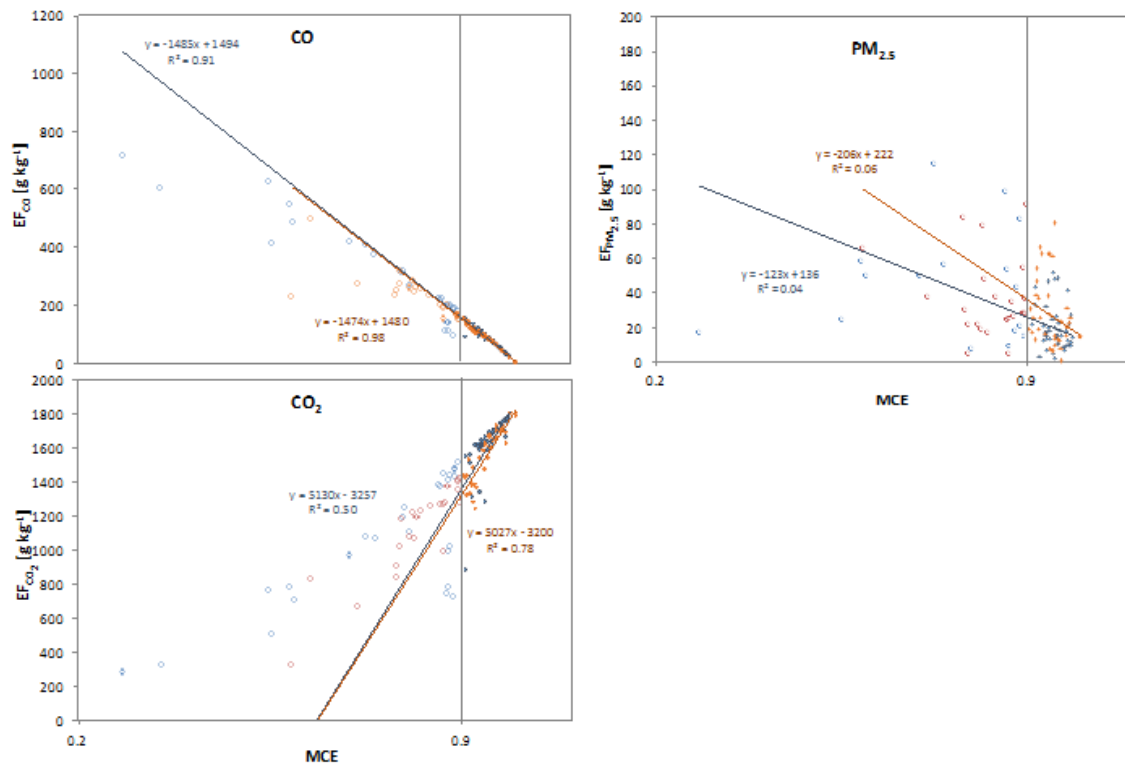
Figure 11. Emission factors for CO, CO_2, ad $PM_{2.5}$ plotted against MCE for burn 3 (blue) and burn 4 (red) along with regression lines and correlations to flaming combustion. Note, an MCE > 0.9 is usually considered the primarily flaming phase while MCE < 0.9 is the primarily smoldering phase.

3.7   Plume rise

Plume rise for burn 3 ranged from 400 m (~1300 ft.) to 1500 m (~5000 ft.) during hand ignition, with an average height of 880 m (~2900 ft.). The mixing height at the start of the burn was 1 km and continued to increase until mid-afternoon.   Smoke emissions continued after hand ignition; however plumes emitted from these sources did not rise above the canopy top. The smoldering emissions did not have the heat and/or energy to transport the plume through the canopy, which acted as a barrier, much like an inversion layer trapping the smoke near the forest floor.

- During mid-day, mid-ignition, the part of the smoke plume that rose above the canopy topped out at the top of the atmospheric mixing layer.

- Results indicate that smoke trapped under the canopy remains near the ground and slowly advects (moves) away from the burn unit and/or drains downhill, which could lead to unintentional smoke impacts.

30

- Stopping the burn and/or emissions earlier in the day would allow for the daytime heating to further assist with diluting the smoke plume and ejecting it from beneath the canopy, thus reducing the potential serious smoke impacts.

3.8   Modeling pathways

The data collected during the prescribed burns were used to evaluate smoke modeling pathways through the BlueSky Framework to find the best 'model' for smoke emissions and dispersion from low intensity burns.

3.8.1 Pre-burn and Consumed Biomass.

Modeled fuels from FCCSv1 overestimated the observed fuels, while FCCSv2 underestimated the observed fuels (Fig. 12). It is interesting that FCCSv2 underestimates the fuel loadings because the FCCSv2 represented the fuel type found in Calloway Forest, "Longleaf pine – Turkey oak forest with prescribed fire" while FCCSv1 misrepresented the fuel type as "Loblolly pine – Short leaf pine – Mixed hardwoods forest".

- FCCSv2 represents fuel loadings as a "snapshot" and for this case, FCCSv2 fuel loadings were too low, representing either a more frequent prescribed fire return interval compared to what was actually practiced, or an interim year between burns.

- The default bulk density of longleaf pine litter within Consume3 is 3 (tons/acre-inch) and this was close to what was found in the field with values ranging from 2.77 tons/acre (burn 1) to 3.87 tons/acre (burn 3) with approximately 1 inch of duff.

The trend of over- and under- estimation persisted in the modeled consumption results. The exception was for burn 3 where the FCCSv1, Consume3 combination produced consumed biomass values near the observations (Fig. 12).
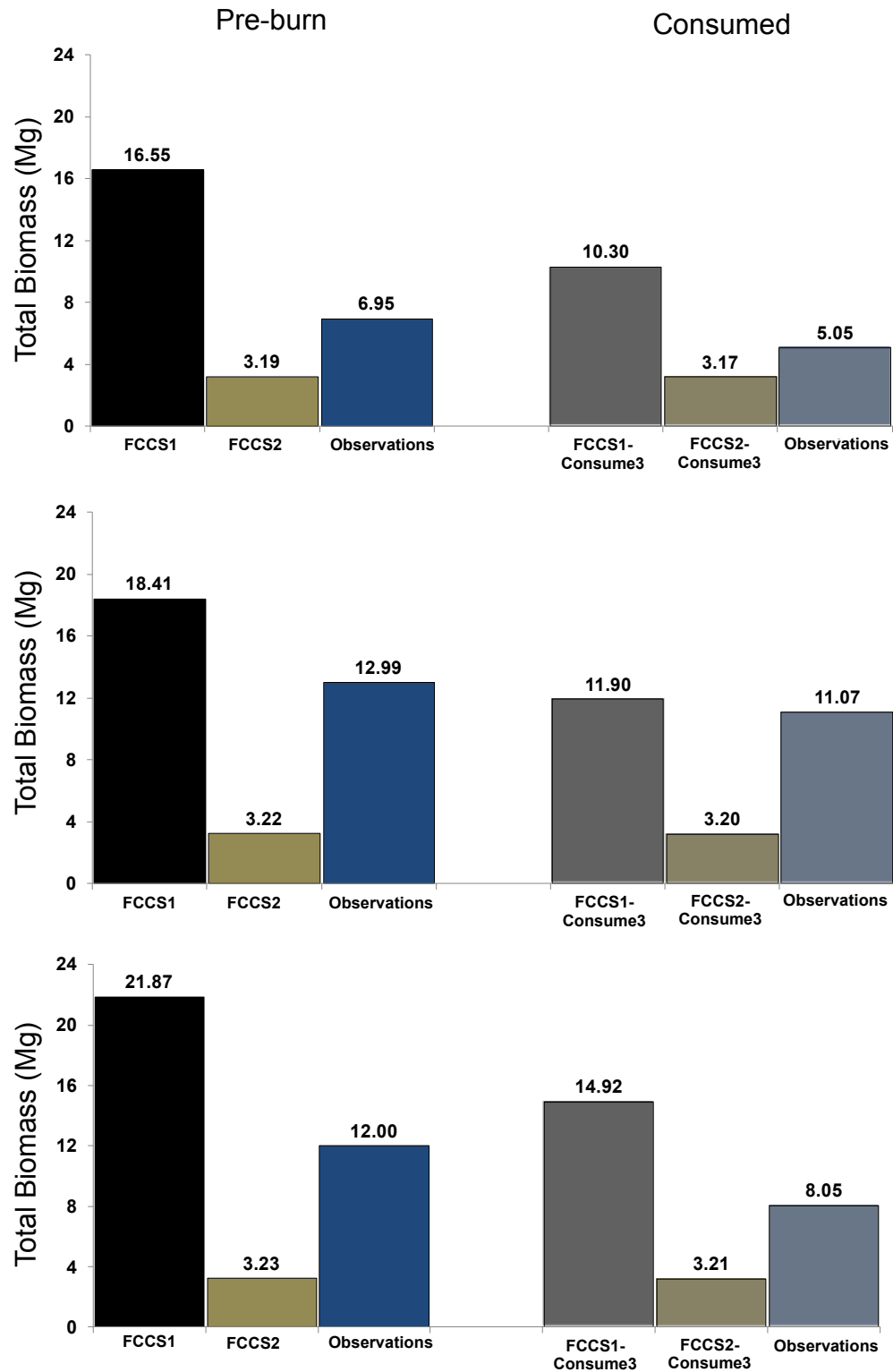
Figure 12. Modeled and observed total fuels/biomass (in Megagrams) before the burn (left side) and total fuels/biomass consumed during the burn (right side) for burn 1, 61 acres (top), burn 3, 175 acres (middle), and burn 4, 225 acres (bottom).

To determine if adding observed fuels would tune the model towards observed consumption, the fuel loads were replaced by observations (Fig. 13). Two methods were used, (*i*), the observed litter class was placed in the model's litter class input field (Tuned F1); and (*ii*), the observed litter class was placed in the model's 1-hr woody fuel class input field (Tuned F2).

- The Tuned F1, Consume3 model combination produced low consumption values compared to the observations.

- Tuned F2 assisted Consume3 and tuned the consumption model towards the consumed observations.

Consume3 handles consumption of litter and 1-hr woody fuels with different algorithms. The 1-hr fuel type for southern fuels is 100% consumed while the litter fuel type is placed into an equation that takes into account forest floor reduction and depth of the litter (Prichard et al., 2010). The complete combustion (100%) of the pine litter, when placed in the 1-hr fuel class, better represented the total consumption observed in the field.
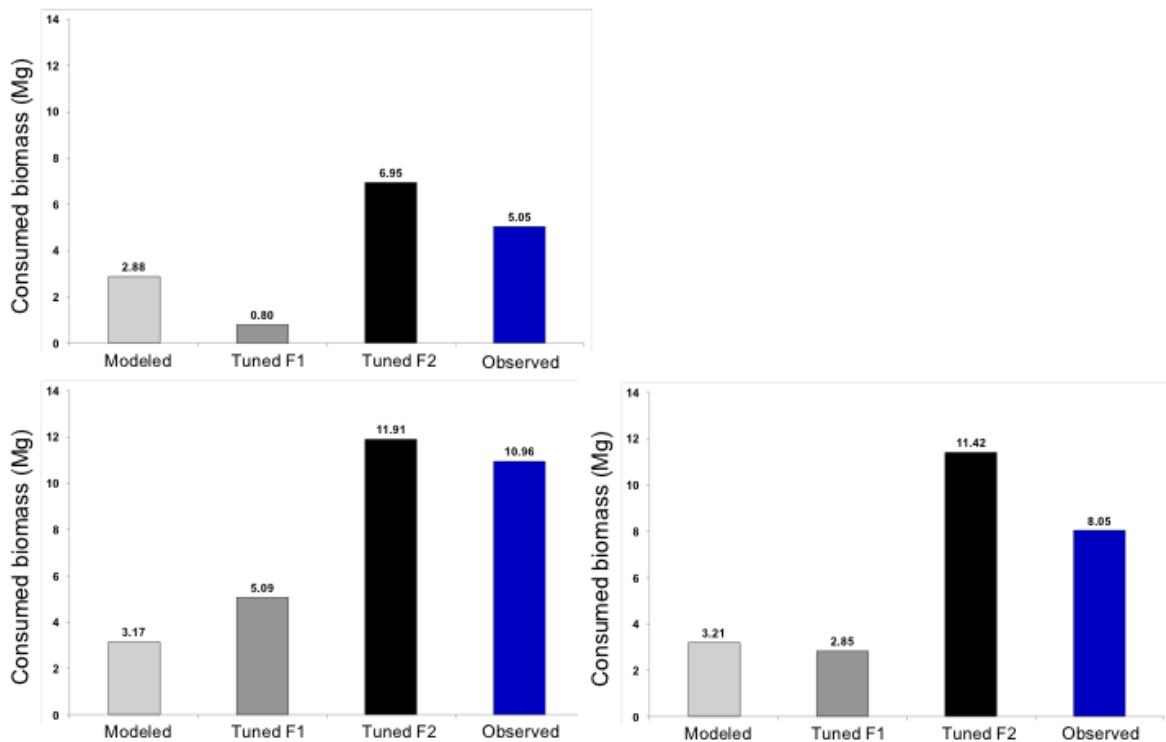

Figure 13. Modeled (FCCSv2, Consumev3), tuned, and observed consumed biomass (in Megagrams) for burn 1 (top left), burn 3 (bottom left), and burn 4 (bottom right). Tuned F1 and F2 are pathways tuned with observed fuels where the litter class is entered as litter (F1) and 1-hr woody fuels (F2).

3.8.2 Emissions.

Modeled PM$_{2.5}$ emissions (FCCSv2, Consume3, FEPS) per unit area (i.e., hectare) were the same for all three burns (Fig. 14). This was the result of the same fuel type, "Longleaf pine – Turkey oak forest with prescribed fire", used by the model for all of the burns. Emissions results varied from burn to burn for the tuned pathways.

Tuned F1 and tuned F2, which used observed fuels, Consume3 and FEPS (for computing emissions), underestimated the observed PM$_{2.5}$ emissions. Observed consumption was entered into the pathway (observed consumption, FEPS) to tune the emissions model (Tuned C) and this combination produced lower emissions than the Tuned F2 pathway. This is interesting because total consumption produced by Tuned F2 was similar to Tuned C (see Fig. 13). The differences in emissions arose from the FEPS emissions model, where the small fraction of smoldering and residual consumption in the Tuned F2 model output strongly influenced the emissions results. For observed consumption, or Tuned C, fraction of consumption in the smoldering and residual phases was unknown and therefore all of the total consumption was placed into the flaming phase. In theory, given the light and flashy fuels this was a good assumption, however in practice, visual inspection and data collection recorded smoldering emissions during and after ignition.

- The differences in emissions output between Tuned F2 and Tuned C highlights the importance of correctly apportioning the fraction of smoldering emissions.

- All pathways, modeled and tuned, underestimated PM$_{2.5}$ emissions ranging from 59% (tuned F2) to 88% (modeled).

- The Tuned F2 pathway provided the closest estimate to the observed emissions (see Section 2.3.5 for how observed emissions were quantified).
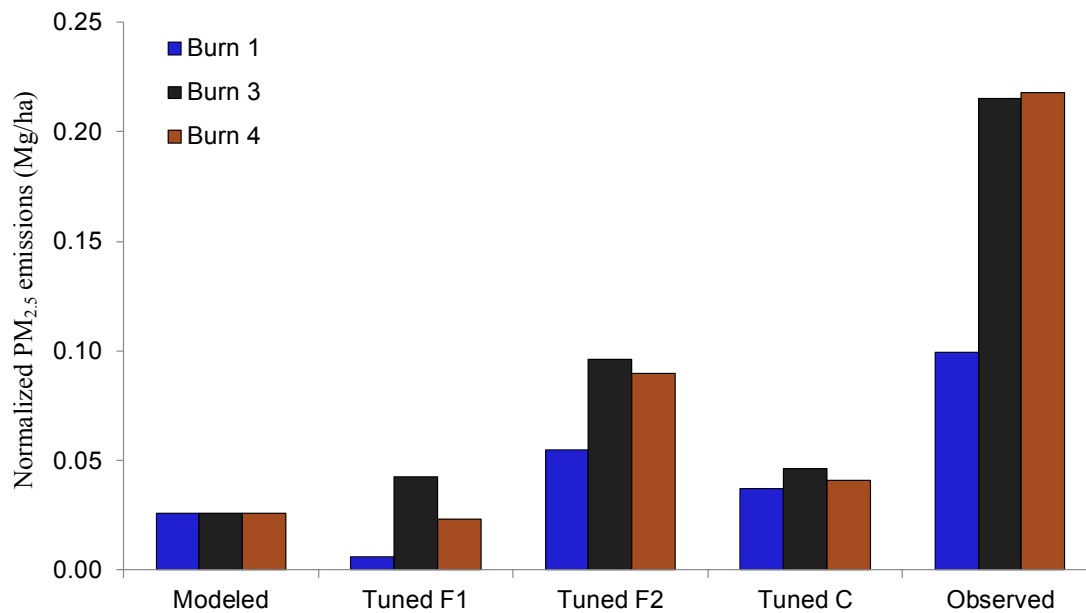
Figure 14. Emissions of PM$_{2.5}$ (Megagrams) normalized by area (hectares). Modeled emissions used the FCCSv2, Consume3, FEPS pathway; Tuned F1 and F2 used observed fuels, Consume3, FEPS pathway; and Tuned C used observed consumed fuels, FEPS pathway. The observed values were calculated using observation derived emission factors and observed fuel consumption.

3.8.3 Plume rise and Dispersion.

Plume rise is an important component in the smoke modeling pathway because it assigns emitted pollutants to each transport layer between the ground and the plume top. The transport layer determines the distance the smoke plume travels and the rate of smoke plume dilution. Misplacement of the smoke plume into the wrong transport layer leads to erroneous surface concentration predictions of smoke.

• Modeled and tuned maximum plume top heights were low relative to the observed maximum plume height (Table 6).

• The observed maximum plume top height reached the top of the mixed layer, which the model did not predict.

Table 6. The maximum plume top height observed, modeled and produced from the tuned pathways for burn 3.

	Modeled	*Tuned F1*	*Tuned F2*	*Tuned C*	*Observed*
Top of the plume (m)	340	450	760	540	1500

35

The modeled and Tuned F2 emissions pathways were used in the BlueSky Framework to compute smoke dispersion. The Tuned F2 pathway was selected for this analysis because it was the model pathway that produced $PM_{2.5}$ emissions closest to the observed emissions. A recent version of the BlueSky Framework (version 3.5) was released during summer, 2013. Included in the new version is the latest version of HYSPLIT (Draxler and Hess, 1997, 1998; Draxler, 1999) as well as the option to utilize HYSPLIT's particle-particle mode, which was previously not available through the BlueSky Framework connection. Examples of surface $PM_{2.5}$ concentrations are shown for burn 3 (Fig. 15).

- The older version of the BlueSky Framework predicted $PM_{2.5}$ concentration values that were comparable to those observed, but not in the correct location.

- The latest version of the Framework (using HYSPLITS particle-particle mode) located the plume correctly, but predicted lower $PM_{2.5}$ concentrations than observed, even when the Tuned F2 model pathway, which produced higher emissions, was invoked.

The placement of the plume in the correct location is a huge step forward in predicting smoke concentrations from low intensity burns. Future model evaluations with the new Framework may lead to model configurations that better quantify surface concentration values. For example, an update of the emission factors algorithms with more recent emissions factors found in the literature would improve the predicted values.

Figure 15. $PM_{2.5}$ surface concentrations at 19:00 EST produced by burn 3 (orange triangle outlines the burn unit). *Left side*, output from the BlueSky Framework v3.0 in use at the time of the burns, with an older version of HYSPLIT and, *right side* output from the v3.5 that includes a new version of HYSPLIT. *Top* panels show surface concentrations produced by the modeled pathway and *bottom* panels show surface concentrations produced by the Tuned F2 pathway. The TG tower was located in the burn unit outlined with yellow. North is the top of the figure.

3.9   Gaussian Modeling

3.9.1 Gaussian line source.

We used the SF_6 tracer data as a basis for testing simple Gaussian plume formulations to treat near-field, in-canopy dispersion. In the first year, we used a simple line source equation and did a sensitivity analysis of the model and comparison to the tracer measurements collected at various heights on the TG tower. For the base case, we used wind speed (WS) = 1 m/s, turbulence in the crosswind direction (sig-V) = 0.5 m/s, turbulence in the vertical direction (sig-w) = 0.2 m/s, the angle of the wind relative to the line source (theta) = 90 deg, and effective height of the emissions (H). We next calculated SF_6 maximum concentrations at the tower using a range of values relative to the base case (Table 7). Changing the sigma V gave the best minimum and maximum modeled results when compared to corresponding observed SF_6 concentrations.

Table 7. Summary of tracer concentrations (ppt) from Gaussian line source modeling for burn 1. Minimum and maximum for the observed SF_6 concentrations, taken from the 5-min concentration data for when the plume was at the TG tower, are shown in the left column. Minimum and maximum concentrations from the sensitivity analyses are shown in the subsequent columns.

	Obs SF6	WS (+-50%)	sigma V (+-50%)	sigma w (+-50%)	theta (90, 60, 30 deg)	H (5 to 35 m)
Minimum	471	339	372	60	332	202
Maximum	592	488	548	440	440	440

We conducted additional model tests for burn 3. In this case, we used the observed meteorological conditions and calculated the average modeled SF_6 concentration at the tower sampling locations. Results are shown in Figure 16 and Table 8.

Overall the line source model results:

- Are in reasonably good agreement with the range of observed concentrations.

- Show less variability compared to the observations but accurately simulated the maximum value.

These analyses indicate that a simple Gaussian line source equation can provide a good prediction of concentrations near the burn.
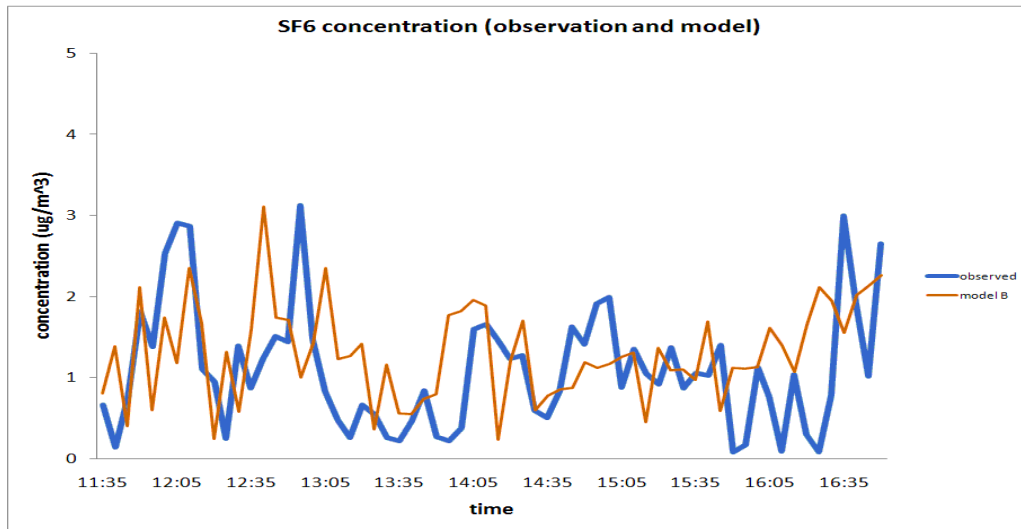
Figure 16. Time series of measured (thicker blue line) and modeled (narrow tan line) SF_6 tracer concentrations averaged over four sampling heights on the TG tower, during burn 3.

Table 8. Summary of model performance statistics for modeling SF_6 tracer concentrations emitted from burn 3.

Performance Measure ($\mu g/m^3$)	Observed	Predicted
Maximum concentration	3.12	3.11
Mean concentration	1.11	1.30
Standard deviation	0.76	0.59

3.9.2 Gaussian puff source.

A Gaussian puff model designed to simulate sub-canopy plume transport (Strand et al., 2009) was used as a virtual laboratory to examine plume rise and dilution of $PM_{2.5}$ concentrations near the fire-source (Fig. 17). The $PM_{2.5}$ released during the 10 minutes it took for the FFP to surround a tower was modeled as a ring-source of $PM_{2.5}$. Sonic anemometer wind data collected at the T1 tower, burn 1, at 3 m (9.8 ft.) AGL were used as input into the model. The model used the wind data to advect the plume downwind, to move the plume vertically, and to calculate the plume dilution due to turbulence.

The puff model helped to demonstrate the vertical motion of the plume (buoyancy) and the extent of plume dilution.   For example, the simulated plume concentrations dropped

38

by a factor of ten between 2.1 m (7 ft.) and 20 m (66 ft.) AGL, the top of the canopy. Given that the model was driven by observed turbulence data, this modeled dilution demonstrates the rapid mixing ongoing directly above the fire.

 Near the surface, a single plume with only one 'core' of concentrated $PM_{2.5}$ concentrations was modeled. At the canopy top, the model simulated two lobes, or 'cores' of higher concentrations. This demonstrates the potential use of the puff model in an operational BlueSky Framework. Diluted plume emissions at the top of the canopy, and their location, as simulated by the puff model, could be used as input at the plume rise step to better describe the quantity of 'emissions' at the canopy top.

The Guassian puff model was used as a virtual laboratory to explore plume rise and dilution directly above the fire. The Gaussian puff model is complex compared to the simple line source model described above. It is good for examining sub-canopy plume dynamics, such as buoyant plume rise and rapid dilution that may otherwise be difficult to observe. Although computationally demanding, the Gaussian puff model demonstrated the potential for modeling sub-canopy fire smoke plumes on fine spatial and temporal scale.   Plume buoyancy was described by using the 10 Hz vertical wind velocity recorded by the sonic anemometer, which was located above the fire front passage. The puff model used the 3-dimensional sonic winds as input. Simulations with estimated winds may not describe plume motion and dilution on a similar fine temporal scale. In general the Gaussian puff model:

- Allowed for virtual exploration of in-canopy plume rise and dilution; and

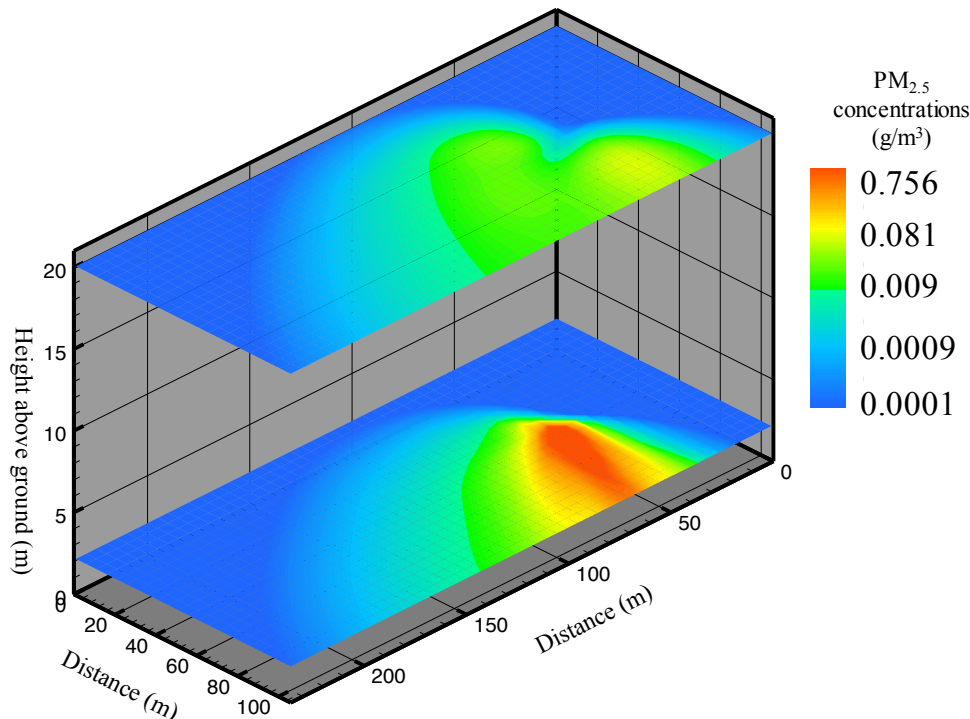- Demonstrated the rapid mixing that occurred at T1 during fire front passage.

Figure 17. Modeled thirty-minute averaged PM$_{2.5}$ concentrations near the T1 tower at 2.1 m (7 ft.) AGL and at the canopy top, 20 m (66.6 ft.) AGL. Particulates were released for ten minutes at the start of the modeling period to simulate the ignition around the tower.

4.   *Management Implications*

Fire Information.

- Incorporating burn manager target start and ending times into the BlueSky Framework on a finer more localized scale (e.g., for TNC it was 11:00 AM start with a hopeful 3:00 PM finish) will improve smoke emissions and predictions. This would capture a more accurate time rate of emissions.

- If management objectives include flame height limitations, this information can be used by the BlueSky Framework to compute consumption efficiency and heat. The difference in flame heights between burn 3 and burn 4 in many ways explains the differences in emissions (tall flames, hotter and more intense fire, different quantities of emitted trace gases).

Fire front passage and turbulence.

- The ground fire increased horizontal winds at the canopy top (20 m, 66 ft. AGL), mid-canopy (10 m, 33 ft.) and at the forest floor. Although winds increased at the

canopy top, the fire mainly affected turbulence and wind between the forest floor and mid-canopy.

▪ Implications of downdrafts that occur mainly within the canopy rather than pulling in air from above-canopy, as found in this study, include the development of warmer sub-canopy conditions, faster pre-heating of the fuels and an increase in the quantity of fuel available for combustion.

▪ Vertical profiles of temperature can assist with studying the impact of fire on the canopy, such as leaf scorch and seed/stem death.

Fuels and consumption.

▪ For these types of fuels and managed burn return interval, using observed fuel loads will not improve the model emissions or dispersion results enough to warrant the expenditure of time to measure fuel loadings.   This should be readdressed when the emission factors algorithms are updated with current values and trends found in the literature.

▪ In predominantly litter fuel beds the fuel moisture of the litter (for Calloway Forest, litter and wiregrass), the primary fuel carrying the fire, will better describe fire behavior and the suite of speciated smoke emissions compared to 1-hr woody fuel moisture content or a fuel-bed average.

▪ Fuels greening after dormancy contribute moisture to the total fuel moisture mosaic and alter the quantity of nitrogen-based emissions.

Emissions.

▪ The emission factors derived from the pollutant concentration measurements during these burns provide new emissions data for prescribed fires and will improve our ability to assess the impact of these low intensity prescribed fires on air quality.

▪ Derived emission factors calculated from concentrations measured in the fire source were similar to those computed from concentrations measured downwind (~500 m) from the fire source.

Smoke concentrations.

▪ All four burns had increased concentrations of $PM_{2.5}$ starting in the early evening (~17:00) and continuing until 24:00. This corresponded to the development of the nocturnal boundary layer, which trapped the smoke near the ground.

▪ Any smoke trapped below the canopy as the nocturnal boundary layer forms (early evening) will remain below the canopy until winds either clear it out or daytime heating increases the depth of the mixing layer.

- An earlier burn time would allow for dilution of the smoldering/residual smoke prior to the development of the nocturnal boundary layer. This would decrease the quantity of particles trapped beneath the canopy.

- The extent of the coupling between the layer below the canopy and the atmospheric layer above the canopy will influence the mixing process and dilution of the smoke plume.

- Canopy cover and stem density are directly correlated to plume dilution and the mixing of air from above canopy to the forest floor (Thistle et al., 2011); both are good proxies for assessing the potential for smoke to remain beneath the canopy once the heat from the fire front passage has dissipated.

Modeling emissions and dispersion.

- The default fuel module within the BlueSky Framework, FCCSv2, underestimated the fuel loadings while FCCSv1 overestimate fuel loadings.

- Using observed fuel loadings with the observed litter loads as woody 1-hr fuel loads, rather than litter (named Tuned F2), produced modeled consumed fuel values that were similar to the observed consumed fuel values.

- Emissions were underestimated by all modeling pathways including Tuned F2, despite Tuned F2 matching the observations in the consumption step.

- The simplest and easiest method to improve smoke emissions predictions (across the country) is to update the emission factors algorithms with recent emission factors and relationships found in the literature. Current emissions factor algorithms (within FEPS) for CO, CO_2, CH_4, and $PM_{2.5}$ use the linear relationships, derived by Ward and Hardy (1991) from Washington, Oregon, and California burns, that associate combustion efficiency to emission factors. Other emission factors within the framework (NOx and NH_3) are static and based on Battye and Battye (2002). Several studies have since improved upon both the linear relationships and the static averages. Framework emissions factors should be updated to reflect the more recent literature.

- Adding an emission factor module to the BlueSky Framework would allow for quicker incorporation of the emissions research into the Framework and into end-user tools used by the air quality and land management decision making communities.

- Maximum modeled plume top height was underestimated compared to that observed in the field and this follows the findings of Raffuse et al. (2012) who found MISR plume tops to be higher than modeled plume tops for small burns.

- The newly released BlueSky Framework, which includes the latest version of HYSPLIT, correctly located the smoke dispersion plume and this was a huge step forward for predicting $PM_{2.5}$ concentrations from low intensity burns. The $PM_{2.5}$ concentrations however, were underestimated.

- For predicting smoke dispersion from low intensity fires, it is recommend that the new version of the BlueSky Framework be used with the following path: observed fuel loads, where the pine litter fuel is placed in the woody 1-hr fuel category, Consumev3, FEPS, and HYSPLIT with the particle-particle option turned on. If fuel loads are not known, or if the fuel type that carries the fire is something other than litter, then FCCSv2 is recommended. Future improvements to the emissions step will hopefully improve the magnitude of the predicted surface concentrations.

- The simple Gaussian line model gave exciting results, demonstrating its use for modeling near-fire smoke concentrations.

5.   Relationship to other recent findings and ongoing work

Throughout the duration of this project we have worked with Dr. Warren Heilman and team (JFSP 09-1-04-1) who did a similar study, albeit with a slightly different focus, in the New Jersey Pine Barrens. We set up our data collection as similar as realistically possible so the data sets could be interchangeable, thus allowing for future exchange and testing of our modeling approaches with data collected in a different environment. Ongoing discussions of results and findings are continuing. In addition, collaboration is ongoig to bring the turbulence data collected under the different forest canopy types, and during different types of burn ignition, together for analyses, comparisons, and hopefully to find trends that are generic enough for use in simplified model algorithms.

Turbulence measurements made during fire front passage were used in combination with previous FireFlux studies that were conducted in grass fields. This early-in-project work helped us to understand the influence of the forest canopy on the turbulence produced by the fire front passage, see Seto et al. (2013) for further details. In addition, ongoing research with the Forest Health Enterprise Technology team (USFS Morganton, WV) continues to progress our understanding of turbulence within a forest canopy and resulting plume dilution. Simple relationships between stem density and downwind concentrations have been developed for a non-buoyant plume.

The case study protocols outlined by the Smoke and Emissions Modeling Intercomparison Project (SEMIP), JFSP 08-1-6-10, were integral in forming this project's experimental design and data collection plan. The SEMIP project found a lack of cohesive data collected from a single burn (fuels, consumption, emissions, etc.). Filling

this data gap was necessary to adequately test the smoke modeling pathways for predicting emissions and dispersion from low intensity burns. When it was realistically possible observation data were collected at each of the smoke modeling output steps.

This project found synergy with *Summary and analysis of approaches linking visual range, PM2.5 concentrations, and air quality health impact indices for wildfires* by O'Neill et al. (2013) and supported publication costs. The topic of the peer reviewed manuscript addresses the combination of water vapor and $PM_{2.5}$ concentrations and how they interact to reduce visibility. This interaction is important for addressing smoke impacts from sub-canopy smoke drift onto highways and to understand conditions that lead to super fog events.

The project *Reducing Uncertainties in Smoke Emissions Modeling* funded by *NASA: Decision Support through Earth Science Research Results* was leveraged for this work. The NASA Decisions funding assisted, in part, with the new release of the BlueSky Framework version 3.5, which was used in these model analyses.

Ongoing research at Washington State University to improve fire emissions in air quality models (AIRPACT) has complimented this work.

6. Future Work Needed

This study found both technical and scientific gaps that future work should strive to close. The technical gaps are:

(i) The emissions factor algorithms and the static emissions factors used within the BlueSky Framework have not been updated with recent values found in the literature, which expand across several fuel types and spatially across the U.S.;

(ii) An e*missions factor* module (different from the *emissions* module) is needed within the Framework. An *emissions facto*r module would allow for easy updates of the emission factors with new research and for addition for local emissions factors.

The scientific gaps are:

(i) Examine the line source model with other case studies (e.g., JFSP 09-1-04-1 data) to further evaluate its potential for prediction near-fire smoke dispersion and if robust, link it operationally into the Framework. This model has the added advantage of being computationally simple and fast and should be compared to other more complex models tested by Heilman et al. (JFSP 09-1-04-1).

(ii)   Bring together the meteorology that forms super fog with $PM_{2.5}$ concentrations. While the meteorological variables that contribute to super fog are understood, little exploration has gone into the combination of meteorology and emissions. Extensive work is ongoing in the southeastern U.S. to predict the potential for super fog (e.g., Achetemier, 2006) and efforts have been made to link super fog formation to heat of combustion, which is a proxy for the emissions, but the heat value is difficult to obtain. Real-time systems exist that are currently predicting both meteorology and $PM_{2.5}$ emissions. We propose that these are combined into an end-user tool (Fig. 18). Where the cut-offs for each category sits (High, Low, etc.) requires further study.

(iii)   Explore methods to operationally run smoke dispersion models on a finer horizontal spatial resolution. A finer horizontal spatial resolution will improve smoke predictions from low intensity burns and drainage of smoke in complex terrain and in terrain with smaller features. This requires stepping away from traditional meteorological and dispersion models.

(iv)   Additionally, we are continuing to collaborate with Dr. Warren Heilman and team (JFSP 09-1-04-1) to incorporate their results into the BlueSky Framework. We are exploring a new pathway in the Framework that will bypass HYSPLIT and send emissions from the Framework into their fine-scale dispersion model. The line source model will also be considered. Additional field studies will be required to determine which models perform better for predicting smoke dispersion from low-intensity burns.

(v)   Further work is necessary to quantify the role of fire-atmosphere interactions on smoke emissions and plume rise and dispersion. Collaboration between the JFSP 09-1-04-1 (Heilman et al.) and JFSP 09-1-4-2 (Strand et al.) research groups is ongoing to jointly examine their turbulence datasets to determine if fire front passage turbulent trends found in one research trial are also found in the other. This is the necessary next step towards finding generic algorithms that can describe fire-atmosphere interactions and smoke emissions.

	Meteorology Super fog Potential[a]			
PM2.5 Emissions Super fog Potential[b]	**Very High**	**High**	**Medium**	**Low**
Very High				
High				
Medium				
Low				

[a]Predicted meteorology is fed into the existing super fog equations (Achtmeier, Curcio's, etc.)
[b]Predicted emissions are generated from models such as BlueSky Playground.

Figure 18. Proposed scaling tool for linking super fog prone meteorology with $PM_{2.5}$ emissions. Where the cut-offs for each category sits (High, Low, etc.) requires study, as does the associated action plan for each color.

7.   *Deliverables*

Table 9 lists the publications and presentations that report the work and results of this project. This work was presented through 9 poster presentations, 7 oral presentations, one classroom lecture, and 3 invited presentations/lectures. In addition the work was presented to land management on 3 different occasions.

The project has produced two master theses, one PhD dissertation, and has assisted in supporting four internships (additional support assistance through the Hispanic Association of Colleges and Universities and American Recovery and Reinvestment Act) and two Research Experience for Undergraduates at Washington State University (student support from the National Science Foundation).

There is currently one peer reviewed paper in publication; two peer reviewed publications that are in submittal draft form; and two peer reviewed publications that are in prep, one of which will summarize the project results through smoke model pathway analyses.

The project has completed all deliverables outlined in the proposal and Table 10 does the crosswalk between deliverables. Data submission to the SEMIP data warehouse is on hold while we wait for instructions.

Table 9. List of published papers and presentations.

Published papers, Masters Theses, PhD Dissertations
Alonso Garcia, F. (2012). Evaluación de las emisiones liberadas por fuegos controlados en el bosque Calloway, North Carolina. *Propuesta de Tesis*. Universidad Metropolitana de Puerto Rico**.**
Seto, D., C. B. Clements, and W. E. Heilman (2013). Turbulence spectra measured during fire front passage. *Agricultural and Forest Meteorology*, 169, 195– 210.
Seto, D. (2012). Observations and Analysis of Fire-Atmosphere Interactions during Fire Front Passage. *Master's Thesis*. San José State University. Paper 4212.
Yedinak, K. M. (2013). Characterization of smoke plume emissions and dynamics from prescribed and wildland fires using high resolution field observations and a coupled fire-atmosphere model. *Doctor of Philosophy Dissertation*. Washington State University.

Papers in preparation
Mickler, R.A. and D. Welch. Pre- and Post-burn fuel loading in a longleaf pine forest following prescribed burning. Proposed journal: *Southern Journal of Applied Forestry, to be submitted*, to be submitted December 2013.
Seto, D., C. B. Clements, T. M. Strand, R. Mickler, and H. Thistle. Turbulence and plume thermodynamic structures during low-intensity subcanopy fires. Proposed journal: *Agricultural and Forest Meteorology*, to be submitted October 2013.
Strand, T. M., V. Cruz Chercon, M. Rorig, K. Yedinak, B. Lamb, and A. Alonso Garcia**.** Evaluating models for low intensity wildland burning using comprehensive observations from four prescribed fires. Proposed journal: *Journal of Geophysical Research-Atmospheres*, to be submitted December 2013.
Strand, T. M., C. Clements, B. Lamb, R. Mickler, M. Rorig, H. Thistle, D. Seto, K. Yedinak, A. Alonso, V. Cruz, P. O'Keefe, G. Allwine, R. Solomon, and X. Bian. Sub-Canopy Smoke Dispersion Study: A unique observation dataset for model development. Proposed journal: *Fire Management Today*, to be submitted December 2013.

Yedinak, K. M., T. M. Strand, and B. K. Lamb. Pollutant emissions from low intensity pine fores prescribed burns. Proposed journal: *Atmospheric Chemistry and Physics*, to be submitted October 2013.

Presentations given to scientific audiences

Allwine, E., P. O'Keefe, R. Grivicke, T. M. Strand, V. Cruz, C. Clements, H. Thistle, and B. Lamb (2011). Near field pollutant and tracer dispersion during a prescribed pine forest burn. Ninth Symposium of Fire and Forest Meteorology, Palm Springs CA., USA, October 18-20, 2012. *Poster Presentation.*

Alonso, F., C. Krull, T. M. Strand, M. Rorig, C. Clements, B. Lamb, R. Mickler, E. Allwine, R. Grivicke, P. O'Keeffe, D. Seto, K. Yedinak, H. Thistle, and A. Trent (2010). Comparison of measured $PM_{2.5}$ data from two Prescribed burns in North Carolina. Third Fire Behavior and Fuels Conference, Spokane Washington, USA, October 25-29, 2010. *Poster Presentation.*

Clements, C. (2011). Meteorology 164: Introduction to fire weather, San José State University, Fall 2011. *Classroom Lecture.*

Hom, J., M. Gallagher, W. Heilman, C. Clements, D. Seto, N. Skowronski, S. Roberts, T. M. Strand, M. Patterson, K. Clark (2010). Smoke modeling and validation field design: CO, PM2.5, CO2 and smoke monitoring, Third Fire Behavior and Fuels Conference, Spokane Washington, USA, October 25-29, 2010. *Poster Presentation.*

Hom, J. L., W. E. Heilman, M. Patterson, K. L. Clark, N. Skowronski, X. Bian, N. Saliendra, M. Gallagher, T. M. Strand, R. Mickler, C. Clements, and D. Seto (2011). Monitoring CO, PM2.5, CO2 from low-intensity fires for the development of modeling tools for predicting smoke dispersion. Ninth Symposium of Fire and Forest Meteorology, Palm Springs CA., USA, October 18-20, 2012. *Poster Presentation.*

Johns, M., E. Allwine, X. Bian, C. Clements, R. Grivicke, C. Krull, N. Larkin, R. Mickler, P. O'Keeffe, M. Rorig, D. Seto, R. Solomon, T. Strand, H. Thistle, K. Yedinak, and B. Lamb (2010). Near field pollutant and tracer dispersion during a prescribed pine forest burn. PNWIS 2010: Training our Future Environmental Professionals, November 3-5, 2010, Missoula Montana, USA. *Oral Presentation.*

Johns, M., E. Allwine, X. Bian, C. Clements, R. Grivicke, P. O'Keefe, C. Krull, N. Larkin, R. Mickler, T. Strand, H. Thistle, M. Rorig, D. Seto, R. Solomon, K. Yedinak, and B. Lamb. (2011). Analysis of pollutant and tracer dispersion during a prescribed forest burn. 91st Annual meeting of the American Meteorology Society. January 22-27, 2011, Seattle Washington, USA. *Poster Presentation.*

Johns, M., E. Allwine, C. Clements, R. Grivicke, P. O'Keefe, T. Strand, H. Thistle, K. Yedinak, and B. Lamb (2010). Analysis of Tracer Dispersion Data during a Prescribed Fire Event. Washington State University Undergraduate Research Symposium. *Poster Presentation.*

Lamb, B. K. (2012). Prescribed and wildland fire impacts on regional air quality. Pan American Advanced Studies Institute Air Quality at the Interface: Mega Cities and Adjacent Agroecosystems, La Plata, Argentina, Aug, 2012. *Invited lecture*.

Mickler, R. and D. Welch (2010). Assessing fuel loading in Longleaf pine forests for the BlueSky Framework. Third Fire Behavior and Fuels Conference, Spokane Washington, USA, October 25-29, 2010. *Oral Presentation*.

Mickler, R. A., T. M. Strand, M. Rorig, C. Clements, and B. Lamb (2012). Sub-Canopy Smoke Dispersion: Measurements of fire-behavior, fuels, consumption, emissions, plume rise and dispersion near and in a prescribed fire-source. 19th Annual International Emission Inventory Conference, Tampa Florida, USA, August 13-16, 2012. *Poster Presentation*.

Seto, D., C. Clements, F. Snively, and W. Heilman (2011). Turbulence velocity spectra and co-spectra measured during fire front passage. Ninth Symposium of Fire and Forest Meteorology, Palm Springs CA., USA, October 18-20, 2012. *Oral Presentation*.

Seto, D., C. Clements, and T. Strand (2012). Observations of atmospheric turbulence within and above canopy layers during low-intensity prescribed fires. 6th Annual SJSU College of Science Research Day, San Jose, CA, May 2012. *Poster presentation*.

Strand, T. M., D. Seto, C. Clements, X. Bian, R. Mickler, E. Allwine, R. Grivicke, P. O'Keeffe, K. Yedinak, B. Lamb, M. Rorig, and C. Krull. (2010). Sub-canopy transport and dispersion of smoke: An o**ve**rview of the observation dataset collection and future model development. Third Fire Behavior and Fuels Conference, Spokane Washington, USA, October 25-29, 2010. *Oral Presentation*.

Strand, T. M., E. Allwine, V. Cruz Chercon, D. Seto, R. Mickler, B. Lamb, R. Solomon, X. Bian, C. Clements, H. Thistle, and M. Rorig (2011). Sub-canopy smoke dispersion: measurements of fire-behavior, fuels, consumption, emissions, plume rise and dispersion near and in a prescribed fire-source. Ninth Symposium of Fire and Forest Meteorology, Palm Springs CA., USA, October 18-20, 2012. *Oral Presentation*.

Strand, T. M. (2011). Micrometeorology, turbulence, and plume dynamics. Scion, NZ Crown Research Institute for Forestry. December 16, 2011. *Invited presentation*.

Strand, T. M., B. Lamb, R. Mickler, M. Rorig, C. Clements, and H. Thistle (2012). Sub-Canopy smoke dispersion: Measurements near and in a prescribed fire-source to improve fire and smoke modelling tools**.** Research Forum, AFAC (Australasian Fire and Emergency Service Authorities Council), Perth, Western Australia, Australia, August 28-31, 2012. *Oral Presentation*.

Strand, T. M., R. Mickler, C. Clements, M. Rorig, H. Thistle, N. Larkin, and B. Lamb (2013). Evaluating models for low intensity wildland burning using comprehensive observations from four prescribed fires. Fourth Fire Behavior and Fuels Conference,

Raleigh North Carolina, USA, February 18-22, 2013. *Oral Presentation*.

Strand, T. M. (2013). BlueSky Framework tools and research. CSIRO, Melbourne Victoria, Australia, March 18, 2013. *Invited presentation*.

Contributors to the presented material include: Gene Allwine, Steve Brown, Craig Clements, Veronica Clifford, Jennifer DeWinter, Narasimhan Larkin, Brian Lamb, Robert Mickler, Patrick O'Keeffe, Sean Raffuse, Miriam Rorig, Dais Seto, Robert Solomon, Dana Sullivan, Harold Thistle

Wu, Y., E. Allwine, X. Bian, C. Clements, R. Grivicke, P. O'Keefe, C. Krull, N. Larkin, R. Mickler, T. Strand, H. Thistle, M. Rorig, D. Seto, R. Solomon, K. Yedinak, and B. Lamb. (2011). Analysis of Pollutant Emissions and Tracer Dispersion during Prescribed Forest Burns. Washington State University Undergraduate Research Symposium. *Poster Presentation*.

Presentations given to management / user group audiences

Strand, T. M. and R. A. Mickler (2011). Sub-canopy smoke dispersion: Measurements of fire behavior, fuels, consumption, emissions, plume rise and dispersion near and in a prescribed fire-source. Presentation to The Nature Conservancy, North Carolina Chapter, Durham North Carolina, USA, October 26, 2011. *Seminar Lecture*.

Contributors to the presented material include: Gene Allwine, Francisco Alonso, Xindi Bian, Veronica Cruz, Craig Clements, Rodrigo Gonzalez, Rasa Grivicke, Narasimhan Larkin, Brian Lamb, Patrick O'Keeffe, Sean Raffuse, Miriam Rorig, Dais Seto, Robert Solomon, Harold Thistle, Bobby Yuhao

Strand, T. M. (2012). Smoke and fire behaviour research and management tools. New Zealand Rural Fire Research Workshop, Rotorua, New Zealand, June 14, 2012.

Contributors to the presented material include: Gene Allwine, Steve Brown, Craig Clements, Veronica Clifford, Jennifer DeWinter, Brian Lamb, Narasimhan Larkin, Robert Mickler, Patrick O'Keeffe, Sean Raffuse, Miriam Rorig, Dais Seto, Robert Solomon, Dana Sullivan, Harold Thistle

Strand, T. M. and Pearce, G. (2013). Modelling rural fires. Electrical Engineering Seminar Series, University of Canterbury, Christchurch, New Zealand, March 22, 2013. *Invited seminar*.

Contributors to the presented material include: Gene Allwine, Craig Clements, Veronica Clifford, Pete Lahm, Brian Lamb, Narasimhan Larkin, Robert Mickler, Mark Moore, Patrick O'Keeffe, Sean Raffuse, Brian Potter, Miriam Rorig, Dais Seto, Robert Solomon, Dana Sullivan, Harold Thistle

Table 10. Project deliverables listed in the proposal and their status.

Deliverable Type	Description	Status
Conference presentation	At major fire conference (e.g. ~~Fire Ecology~~, Third Fire Behavior and Fuels Conference)	Complete
Non-refereed publication	JFSP annual report	Complete
Preliminary observed data	Data from field campaign (1) compiled and available to team members	Complete
Non-refereed publication	~~In a wildland fire community journal (e.g. fire management today)~~ Seminar lecture: to The Nature Conservancy, North Carolina Chapter, Durham North Carolina, USA, October 26, 2011. *Seminar Lecture*. Note: Strand and Heilman (JFSP 09-1-04-1) in discussion for presenting their work jointly in FMT	Complete
Oral presentation	At major conference (e.g. Ag. and Forest Met.)	Complete
Preliminary simulated data	Preliminary model performance analyses available to team members	Complete
Poster presentation	At major international conference (e.g. AGU Fall Meeting)	Complete
Non-Refereed Publication	JFSP annual report	Complete
International presentation	~~Integrated Land-Atmosphere Processes Study (iLEAPS) meeting~~ International Emission Inventory Conference; 4th fire behavior and fuels conference	Complete
Preliminary observed data	Data from field campaign (2) compiled and available to team members	Complete
Two refereed publications	1) 'Turbulence spectra measured during fire front passage' 2) 'Pollutant emissions from low intensity pine forest prescribed burns'	Complete See publications listed above
Model analysis	Model performance analysis submitted to the group for discussion	Complete
Submission of data to SEMIP	Enter the observed and simulated datasets and evaluation results	Ready for submission, waiting for instructions

Refereed publication	'Evaluating models for low intensity wildland burning using comprehensive observations from four prescribed fires' **Note**: This paper could not be completed until all else was finished.	Strand et al. (in prep); On time
Non-Refereed Publication	Final Report to JFSP	Complete
Conference Presentations	Additional round of conference presentations on results	Complete

Acknowledgements

References

Achtemeier, G. L. (2006). Measurements of moisture in smoldering smoke and implications for fog. *Int*. *J*. *of Wildland Fire*, 15, 517-525.

Akagi, S. K., Yokelson, R. J., Wiedinmyer, C., Alvarado, M. J., Reid, J. S., Karl, T., Crounse, J. D., & Wennberg, P. O. (2011). Emission factors for open and domestic biomass burning for use in atmospheric models, *Atmos*. *Chem*. *Phys*., 11, 4039–4072.

Alonso-Garcia, F. (2012). Evaluación de las emisiones liberadas por fuegos controlados en el bosque Calloway, North Carolina. *Propuesta de Tesis*. Universidad Metropolitana de Puerto Rico**.**

Alexander, M. E. (1982). Calculation and interpreting fire intensities. *Can*. *J*. *Botany*, 60, 349-357.

Anderson, G. K., Sandberg, D. V., & Norheim, R. A. (2004). Fire emission production simulator (FEPS). User's Guide. Available at http://www.fs.fed.us/pnw/fera/feps/FEPS_users_guide.pdf.

Battye, W. and Battye, R. (2002). Development of Emissions Inventory Methods for wildland Fire. *U*.*S*. *Environmental Protection Agency Contract* No. 68-D-98-046

Bisson, P. A, Rieman, B. E., Luce, C. Hessburg, P. F., Lee, D. C., Kershner, J. L., & Gresswell, R. E. (2003). Fire and aquatic ecosystems of the western USA: current knowledge and key questions. *Forest Ecol*. *Manag*., 178, 213-229.

Burling, I. R., Yokelson, R. J., Akagi, S. K., Urbanski, S. P., Wold, C. E., Griffith, D. W. T., Johnson, T. J., Reardon, J., & Weise, D. R. (2011). Airborne and ground-based

measurements of the trace gases and particles emitted by prescribed fires in the United States, *Atmos. Chem. Phys.*, 11, 12197–12216.

Chen, J., Vaughan, J., Avise, J., O'Neill, S., & Lamb, B. (2008). Enhancement and evaluation of the AIRPACT ozone and PM2.5 forecast system for the Pacific Northwest. *J. Geophys. Res.-Atmos.*, 113, 1984–2012.

Draxler, R. R. and Hess, G. D. (1997): Description of the HYSPLIT_4 modeling system. NOAA Tech. Memo. ERL, ARL-224, NOAA Air Resources Laboratory, Silver Spring, MD, *24 pp.*

Draxler, R.R. and Hess, G. D. (1998): An overview of the HYSPLIT_4 modeling system of trajectories, dispersion, and deposition. *Aust. Meteor. Mag.* 47, 295-308.

Draxler, R.R. (1999). HYSPLIT4 user's guide. NOAA Tech. Memo. ERL, ARL-230, NOAA Air Resources Laboratory, Silver Spring, MD.

Dudhia, J. (1989). Numerical study of convection observed during winter monsoon experiment using a mesoscale two-dimensional model. *J. Atmos. Sci.*, 46, 3077-3107.

Dudhia, J (1996), A multi-layer soil temperature model for MM5. Preprints, *6th PSU/NCAR Mesoscale Model User's Workshop, 22-24 July, 1996, Boulder, CO*, pp 49-50.

Ferek, R. J., Reid, J. S., Hobbs, P. V., Blake, C. R., & Liousse, C. (1998). Emission factors of hydrocarbons, halocarbons, trace gases and particles from biomass burning in Brazil, *J. Geophys. Res.-Atmos.*, 103, 32107–32118.

Grell G. A., Dudhia, J., & Stauffer, D. R. (1994). A description of the fifth- generation Penn State/NCAR mesoscale model (MM5). Mesoscale and microscale meteorology division, National Centre for Atmospheric Research. NCAR Technical Note, NCAR/TN-398+STR. (Boulder, CO).

Glitzenstein, J. S., Streng, D. R., & Wade, D. D. (2003). Fire frequency effects on longleaf pine (*Pinus palustris* P. Miller) vegetation in South Carolina and northeast Florida, USA. *Notes*.

Janjic, Z. I. (1990). The step-mountain coordinate: Physical package. *Mon. Wea. Rev.*, 118, 1429-1443.

Janjic, Z. I. (1994). The step-mountain eta coordinate model: Further development of the convection, viscous sub-layer, and turbulent closure schemes. *Mon. Wea. Rev.*, 122, 927-945.

Janjic, Z. I. (2003). A non-hydrostatic model based on a new approach. *Meteor. Atmos. Phys.*, 82, 271-285.

Komarek, E. V. (1974). Effects of fire on temperate forests and related ecosystems: southeastern United States. In: Fire and Ecosystems. Academic Press, New York, pp. 251-277.

Larkin, N. K., O'Neill, S. M., Solomon, R., Raffuse, S., Strand, T., Sullivan, D. C., & Ferguson, S. A, (2010). The BlueSky Smoke Modeling Framework. *Int. J. of Wildland Fire*, 18, 906-920.

Larkin, N. K., Strand, T. M., Drury, S. A., Raffuse, S. M., Solomon, R. C., O'Neill, S. M., Wheeler, N., Huang, S. M., Rorig, M., & Hafner, H. R. (2012). Smoke and Emissions Model Intercomparison Project (SEMIP): Creation of SEMIP and evaluation of current models. *Final report to the joint fire science program*, Project #08-1-6-10.

Liu, Y. (2004). Variability of wildland fire emissions across the contiguous United States. *Atmos. Environ.*, 38, 3489-3499.

Kain, J. S., and Fritsch, J. M. (1990). A one-dimensional entraining/detraining plume model and its application in convective parameterization. *J. Atmos. Sci.*, 47, 2784–2802.

McKenzie, D., Raymond, C. L., Kellogg, L. K. B., Norheim, R. A., Andeu, A. G., Bayard, A. C., Kopper, K. E., & Elman E. (2007). Mapping fuels at multiple scales: Landscape application of the fuel characteristic classification system. *Can. J. Forest Res.* 37, 2421-2437.

Mlawer, E. J., Taubman, S. J., Brown, P. D., Iacono, M. J., & Clough, S. A. (1997). Radiative transfer for inhomogeneous atmosphere: RRTM, a validated correlated-k model for the long-wave. *J. Geophys. Res.*, 102, 16663-16682.

O'Neill, S. M., Lahm, P. W., Fitch, M. J., & Broughton, M. (2013). Summary and analysis of approaches linking visual range, PM2.5 concentrations, and air quality health impact indices for wildfires. *JAWMA*, 63, 1083-1090.

Pearce, H. G., Anderson, S. A. J., & Clifford, V. (2012). A manual for prediction fire behaivour in New Zealand fuels, 2nd edition. Scion, Rural Fire Research Group, Christchurch, New Zealand.

Prichard, S. J., Ottmar, R. D., & Anderson, G. K. (2010). *Consume 3.0 User's Guide.* Pacific Wildland Fire Sciences Laboratory. USDA Forest Service, Seattle, Washington.

Raffuse, S. M., Craig, K. J., Larkin, N. K., Strand, T. M., Sullivan, D. C., Wheeler, N. J. M., & Solomon, R. (2012) An evaluation of modeled plume injection height with satellite-derived observed plume height. *Atmosphere*, 3, 103-123.

Scire, J. S., Strimaitis, D. G., & Yamartino, R. J. (2000). A user's guide for the CALPUFF dispersion model (Version 5). EarthTech, Inc., Concord, MA.

Seto, D. (2012). Observations and analysis of fire-atmosphere interactions during fire front passage. *Master's Thesis*. San José State University. Paper, 4212.

Seto, D., Clements, **C. B.,** & Heilman, W. E. (2013). Turbulence spectra measured during fire front passage. *Agr. and Forest Meteorol.,* 169**,** 195– 210.

Seto, D., Clements, C. B., Strand, T. M., Mickler, R., & Thistle, H. W. (in preparation): Turbulence and plume thermodynamic structures during low-intensity sub-canopy fires, *Agr. and Forest Meteorol.,* to be submitted October 2013.

Strand, T. M., Lamb, B., Thistle, H., Allwine E., & Peterson, H. (2009). A simple model for simulation of insect pheromone dispersion within forest canopies. *Ecol. Model.,* 220, 640- 656.

Strand, T. M., Larkin, N., Rorig, M., Krull, C., & Moore, M (2011). PM2.5 Measurements in wildfire smoke plumes from fire seasons 2005–2008 in the Northwestern United States. *J. Aerosol Sci.,* 42, 143-155.

Strand, T. M., Larkin, N., Craig, K. J., Raffuse, S., Sullivan, D., Solomon, R, & Pryden, D. (2012). Analyses of BlueSky Gateway PM2.5 predictions during the 2007 southern and 2008 northern California fires. *J. Geophys. Res.-Atmos.,* 117, 1984–2012.

Thistle, H. W., Strom, B., Strand, T., Peterson, H. G., Lamb, B. K., Edburg, S., & Allwine, G. (2011). Atmospheric dispersion from a point source in four southern pine thinning scenarios: basic relationships and case studies, *T. ASABE* Vol. 54, 1219-1236.

Urbanski, S. P., Hao, W. M., & Baker, S. (2008). Chemical composition of wildland fire emissions. *Dev. in Environm. Sci.,* 8, 79-107.

Ward D. E. and Hardy C. C. (1991). Smoke emissions from wildland fires. *Environ. Int.,* 17, 117-134.

Ward, D. E. and Radke, L. F. (1993). Emissions measurements from vegetation fires*:* A comparative evaluation of methods and results, pp. 53–76. [online] Available from: http://www.treesearch.fs.fed.us/pubs/40604 (Accessed 2 August 2013).

Yedinak, K. M (2013). Characterization of smoke plume emissions and dynamics from prescribed and wildland fires using high resolution field observations and a coupled fire-atmosphere model. *Doctor of Philosophy Dissertation.* Washington State University.

Yedinak, K. M., Strand, T. M., & Lamb, B. K. (in preparation) Pollutant emissions from low intensity pine fores prescribed burns. *Atmos. Chem. and Phys.,* to be submitted October 2013.

Yokelson, R. J., Goode, J. G., Ward, D. E., Susott, R. A., Babbitt, R. E., Wade, D. D., Bertschi, I., Griffith, D. W. T., & Hao, W. M. (1999). Emissions of formaldehyde, acetic acid, methanol, and other trace gases from biomass fires in North Carolina measured by airborne Fourier transform infrared spectroscopy, *J. Geophys. Res.-Atmos.,* 104, 30109–30125.

Appendix A: Conversion table to convert metric units into US customary system of units.

Metric name	*Metric unit*	*Conversion to US standard units*
Length, Height	1 m	3.3 ft
Length, Height	1 km	0.62 miles
Burn unit area	1 ha (hectare)	2.47 acres
Mass (i.e., fuel loading)	1 Mg	1.1 ton
Emissions	1 g/kg	2 lb/ton
Mass per area	1 kg/ha	0.0004 ton/acre
Wind velocity	1 m s^{-1}	2.2 mph

Appendix B: Instrumentation used in the experimental burns to measure micrometeorology, winds and turbulence during fire front passage, and trace gas and particulate concentrations in smoke plumes.

Location	Measured variable	Instrument	Sampling rate	Manufacturer information	Number deployed	Sampling height
M1, M2	Vertical and Horizontal wind speed and Wind direction	models 5431, 024, and 010C	1Hz	MetOne, Grants Pass, Oregon	2	1m, 7m
M1, M2	Temperature and Relative humidity	model 41372/43372	1Hz	R.M. Young, Traverse City, Michigan	2	1m, 7m
M1, M2	Net radiation	net radiation	1Hz	REBS, Seattle, Washington	2	1m
SODAR	Temperature	radiosonde	1Hz	GRAW Radiosondes, Nuremberg, Germany	1	0-10km
SODAR	Potential temperature	radiosonde	1Hz	GRAW Radiosondes, Nuremberg, Germany	1	0-10km
SODAR	Wind speed and direction	radiosonde	1Hz	GRAW Radiosondes, Nuremberg, Germany	1	0-10km
SODAR	Wind speed + direction	SODAR	15 min	Scintech Corp., Louisville, Colorado	1	0 to 200 m AGL
SODAR	Temperature	SODAR	15 min	Scintech Corp., Louisville, Colorado	1	0 to 200 m AGL
T1	Turbulence/3-d wind	3-d sonic anemometer	10Hz	Applied Technology, Inc., Boulder, Colorado	3	3m, 10m, 20m
T2	Turbulence/3-d wind	3-d sonic anemometer	10Hz	2 x Sx-probe. (3m, 10m) Applied Technology, Inc., Boulder Colorado; 1 x 81000 (20m) R.M. Young, Traverse City, Michigan	3	3m, 10m, 20m
T2	Fine scale temperature	thermocouple	5Hz	5SC-TT, Omega Inc. , Stamford, Connecticut	20	every meter from 0 m to 20 m AGL
T2	Water vapor	krypton hygrometer	10Hz	KH20, Campbell Scientific, Logan, Utah	1	10m
T2	Radiant heat flux	total and radiant heat flux sensors	1Hz	Hukseflux SBG-01(total), Medtherm Model 64 (radiant)	1	1m
T2	BC	micro aethalometer	1Hz	Magee Scientific AE-51	1	10m
T2	PM2.5	dusttrak2	1Hz	TSI, Shoreview Minnesota	1	10m
TG	CO_2	open path IRGA	10 Hz	LI-COR, Lincoln, Nebraska	1	25.6 m
TG	CO_2	cavity ring down spectrometer (CRDS)	10 Hz	Picarro Inc., Santa Clara, California	1	25.6 m
TG	CO_2	closed path IRGA using TGAPS manifold	1 Hz	LI-COR, Lincoln, Nebraska	1	25.6 m, 19.7 m, 7.6 m, and 2.7 m
TG	CO	CRDS	10 Hz	Los Gatos Research, Mountain View, California	1	25.6 m

TG	CH4	CRDS	10 Hz	Picarro Inc., Santa Clara, California	1	25.6 m
TG	NOx	chemiluminescence NOX	1 Hz	Teco	1	1.8 m
TG	NO	chemiluminescence NOX	1 Hz	Teco	1	1.8 m
TG	NO2	chemiluminescence NOX	1 Hz	Teco	1	1.8 m
TG	NH3	CRDS	1 Hz	Picarro Inc., Santa Clara, California	1	25.6 m
TG	PPAH	PAS-PC	5-min	EcoChem Analytics, 2000.	1	1.8m
TG	BC	aethalometer	1Hz	Magee Scientific rackmount (AE-31)	1	1.8m
TG	H2O	open path IRGA	10 Hz	LI-COR, Lincoln, Nebraska	1	25.6 m
TG	Turbulence	3-d sonic anemometer	10 Hz	1 x CSAT3 Campbell Scientific, Logan, Utah; 3 x Applied Technology, Inc., Boulder, Colorado	4	25.6 m, 19.7 m, 7.6 m, and 2.7 m
TG	Temperature (Profiler)	custom made	1 Hz	Climatronics system, Bohemia, New York	8	5.4, 19.3, 17.3, 13.3, 9.7, 7.2, 5.2, and 2.2 m
TG	PM2.5	Environmental Beta Attenuation Monitor	5-min, hourly	MetOne, Grants Pass, Oregon	4	1.8 m
TG	PM2.5	E-Sampler	5-min, hourly	MetOne, Grants Pass, Oregon	1	1.8 m
TG	PM2.5	nephelometer	2 min	Optec, Inc. NGN-3a	1	1.8 m
CO_interior	CO	UC calibrated	1-min	Specially made and calibrated	7	2 m
CO_interior	CO	EL-USB-CO	1-min	Lascar Electronics Ltd, Salisbury, UK	5	2 m

Appendix C: Further discussion on $PM_{2.5}$ concentrations and the E-Sampler and EBAM instruments used to obtain the data.

Concentrations of $PM_{2.5}$ were monitored and recorded on the downwind perimeter of the burn units (burns 1, 2, and 3) to obtain data near the fire source. The burns occurred on 7-Mar-2010, 9-Mar, 2010, 16-Feb-2011, and 12-Mar-2011. For burn 4 the monitors were located inside the burn unit, thus obtaining concentrations inside the fire-source. The pattern of observed $PM_{2.5}$ concentrations was similar across all four experimental burns and can be divided into three phases: initial peak, concentration fluctuations, and elevated nighttime concentrations (Fig. C1).

The initial concentration peak occurred when burn ignition was close to the monitor locations, and for burns 1 and 4 this was when the maximum was recorded. Concentration fluctuations occurred as ignition progressed away from the monitors and were caused by plume meander and dilution. Concentrations began to increase again between 17:00 and 18:00, shortly after ignition ceased, and remained elevated, ranging in the hundreds to low thousands ($\mu g/m^3$), until 24:00. For burns 2 and 3, maximum $PM_{2.5}$ concentrations were recorded during this period. For all burns, during this phase, the monitors recorded similar levels of $PM_{2.5}$ concentrations and trends, increasing and decreasing at nearly the same time.   This suggests the monitors were in a horizontally well-mixed layer of smoke. $PM_{2.5}$ concentrations and their trends measured during all four burns are described by Alonso Garcia (2012).

For burns 3 and 4 two types of monitors were used, the EBAM and the E-Sampler. Trent (2006) compared the EBAM and the E-Sampler to the U.S. EPA gravimetric Federal Reference Method (FRM) in laboratory studies and found the EBAM to measure $PM_{2.5}$ concentrations 1% higher than the FRM and the E-Sampler to measure 8% to 15% higher than the FRM. Strand et al. (2011) found 24-hr averaged (from hourly data) E-Sampler data 3% higher than EBAM data, when co-located and sampling wildfire smoke over several weeks. This was an important addition to the comparison studies because it occurred in the field, for a prolonged period with exposure to elevated concentrations of wildfire smoke, rather than for a 1-2 day period in laboratory conditions. The very high concentration data collected during this Sub-canopy study were observed near the fire-source and understanding instrument performance at high levels of $PM_{2.5}$ further adds to the previous work.

 For this study, the E-Sampler tracked well with the E-BAM during the initial concentration peaks (burns 3 and 4), however during the concentration fluctuations of burn 4 it recorded higher concentrations compared to the other EBAMs located nearby. For both burns during the nighttime fluctuations the E-Sampler measured higher $PM_{2.5}$ concentrations majority of the time compared to the EBAMs.

The EBAM data from burn 3 have a moderate-high positive correlation with each other and each recorded a concentration value similar in magnitude, indicating a plume of evenly mixed smoke over the spatial distance of 200 m (Fig. C2). The E-Sampler, located within this 200 m of evenly mixed smoke recorded higher concentrations than the EBAM data, although the EBAM data also have a moderate-high positive correlation to the E-Sampler data (Fig. C3). The moderate-high positive correlation is due a similar trend in the rise and fall of concentrations recorded by the instruments. At high concentrations, on the order of 400 to 500 $\mu g/m^3$ and greater, the E-Sampler and EBAM diverge (Fig. C3). This however may not be an issue as the U.S. EPA NAAQS for $PM_{2.5}$ is a 24-hr average of 35 $\mu g/m^3$ and previous work (Trent, 2006; Strand et al., 2011) have found the E-Sampler to vary only slightly from the EBAM in those concentration ranges.
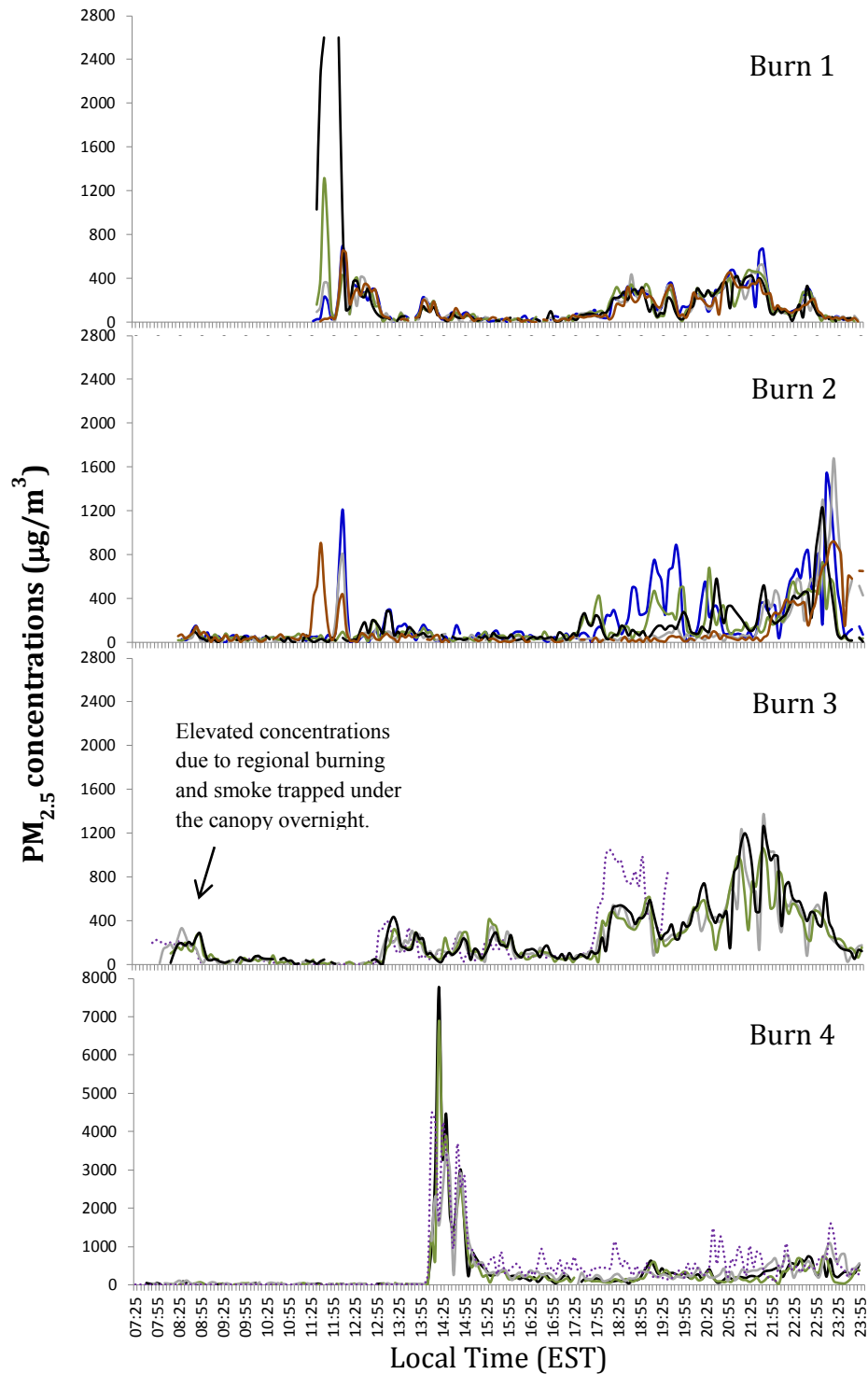
Figure C1. PM$_{2.5}$ concentrations ($\mu g/m^3$) recorded by the EBAM instruments located on the downwind perimeter of the fire (burns 1, 2, and 3) and within the fire (burns 4, note the different Y axis). For burns 3 and 4 the purple dashed line represents concentrations recorded by the E-Sampler. Ignition started at 11:20, 11:00, 11:00, 11:10 for burns 1, 2, 3, and 4, respectively, and ended at 15:20, 14:45, 17:00, and 15:00, respectively. The initial peak was when the fire was near the monitors. This was followed by concentration fluctuations and then the elevated nighttime concentration phase, which began between 17:00 and 1800.
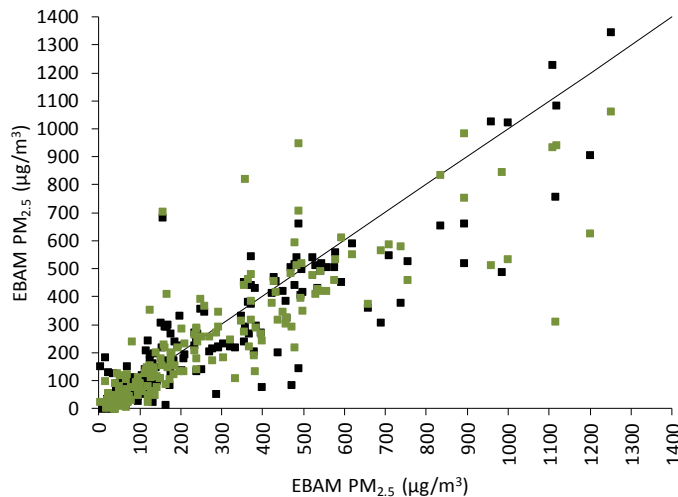
Figure C2. PM$_{2.5}$ concentrations (µg/m^3) recorded during burn 3 by two EBAMs plotted against data recorded by a third EBAM. The EBAMs were spread out over a spatial distance of 200 m. The narrow scatter about the 1:1 line illustrates a well-mixed plume over the horizontal distance.
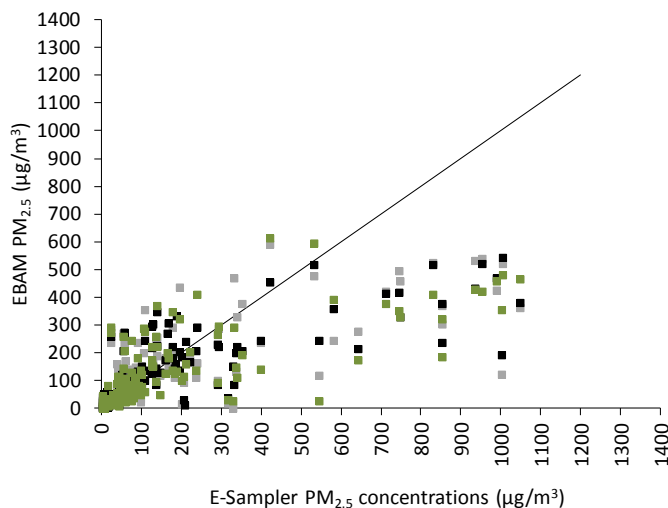

Figure C3. PM$_{2.5}$ concentrations (µg/m^3) recorded during burn 3 by the three EBAMs plotted against data recorded by the E-Sampler. The E-Sampler was located within the 200 m spatial distance noted in Fig. C2 and should have recorded similar values. The data are scattered below the 1:1 line indicating that the E-Sampler recorded higher concentrations than the EBAMs.

References

Alonso-Garcia, F. (2012). Evaluación de las emisiones liberadas por fuegos controlados en el bosque Calloway, North Carolina. *Propuesta de Tesis*. Universidad Metropolitana de Puerto Rico**.**

Strand, T. M., Larkin, N., Rorig, M., Krull, C., and Moore, M. (2011). PM2.5 Measurements in wildfire smoke plumes from fire seasons 2005–2008 in the Northwestern United States. *J. Aerosol Sci.*, 42, 143-155.

Trent, A. (2006). Smoke particulate monitors: 2006 update. Technical Report 0625-2842-MTDC (14 pp.). U.S. Department of Agriculture Forest Service, Missoula Technology and Development Center, Missoula, Montana.